Basin Research (2014) **26**, 1–21, doi: 10.1111/bre.12062

Sedimentary and structural record of the Albian growth of the Bakio salt diapir (the Basque Country, northern Spain)

Y. Poprawski,* C. Basile,* L. Agirrezabala,† E. Jaillard,* M. Gaudin‡ and T. Jacquin‡

*ISTerre, Grenoble CEDEX 9, France

†Estratigrafia eta Paleontologia Saila, Euskal Herriko Unibertsitatea UPV/EHU, Bilbo, The Basque Country, Spain

‡Geolink, Meylan, France

ABSTRACT

However salt has a viscous rheology, overburden rocks adjacent to salt diapirs have a brittle rheology. Evidence of deformation within the overburden has been described from diapirs worldwide. Gravity-driven deposits are also present along the flanks of several diapirs. The well-known example from the La Popa Basin in northern Mexico shows that such deposits may be organized into halokinetic sequences. This leads to several questions: (i) How does diapir growth contribute to overburden deformation? (ii) Are halokinetic sequence models valid for other areas beyond the La Popa Basin. The Bakio diapir and its well-exposed overburden in Basque Country, Spain provides key elements to address these questions. The Bakio diapir consists of Triassic red clays and gypsum and is flanked by synkinematic middle to upper Albian units that thin towards the diapir. The elongate diapir parallels the Gaztelugatxe normal fault to the NE: both strike NE–SW and probably formed together during the middle Albian, as synkinematic units onlap the fault scarp. The diapir is interpreted as a reactive diapir in response to middle Albian motion on the Gaztelugatxe fault. The rate of salt rise is estimated to be about 500 m Myr^{-1} during this passive stage. During Late Albian, the diapir evolved passively as the Gaztelugatxe fault became inactive. Synkinematic units thinning towards the diapir, major unconformities, slumps and other gravity-driven deposits demonstrate that most deformation related to diapir growth occurred at the sea floor. Halokinetic sequences composed of alternating breccias and fine-grained turbidites recorded cyclic episodes of diapir flank destabilization. This work provides insights into drape fold and halokinetic sequence models and offers a new simple method for estimating rates of diapir growth. This method may be useful for outcrop studies where biostratigraphical data are available and for other passive diapirs worldwide.

INTRODUCTION

Steep, vertical or even overturned strata associated with thinning of strata towards growing salt features are commonly described adjacent to diapir walls (e.g. Jackson *et al.*, 1994; Alsop *et al.*, 2000; Giles & Lawton, 2002; Rowan *et al.*, 2003; Schultz-Ela, 2003; Banham & Mountney, 2013a,b,c). Such structures are related to overburden deformation during diapir growth and are commonly difficult to study. In the field, late dissolution of evaporite masses (commonly gypsum or halite) often triggers collapse of the adjacent overburden (e.g. Jackson *et al.*, 1998). On seismic lines, resolution is generally poor near diapir walls because of steep dipping beds, faulted strata, overhanging salt, extreme stratigraphical thickness changes and poor velocity control (Davison *et al.*, 2000). Two different models have been proposed to explain these structures found along diapir flanks (Fig. 1): drag fold (Jackson & Talbot, 1991; Jackson *et al.*, 1994) and drape fold models (Schultz-Ela, 2003). Drag folds involve shearing, folding and faulting of the overburden by evaporite rise with deformation at depth. Drape folds correspond to folding at the basin floor due to differential vertical motion between the diapir and its overburden. Vertical motions of the basin floor may create sedimentary sequences controlled by the balance between the rates of diapir rise and adjacent sedimentation. Such halokinetic sequences have been described in the El Papalote diapir (La Popa basin, northern Mexico; Giles & Lawton, 2002; Rowan *et al.*, 2003).

This paper presents field-based sedimentological and structural analyses from the Bakio diapir in the Basque–Cantabrian Basin. The Bakio overburden displays syndiapir growth strata, well-exposed sedimentary wedges that

Correspondence: Y. Poprawski, ISTerre, BP 53, Grenoble CEDEX 9 38041, France. E-mail: yohann.poprawski@gm.univ-montp2.fr

BRE | 12062 | WILEY | Dispatch: 19.2.14 | CE: Supriya
Journal Code | Manuscript No. | No. of pages: 21 | PE: Murugavel

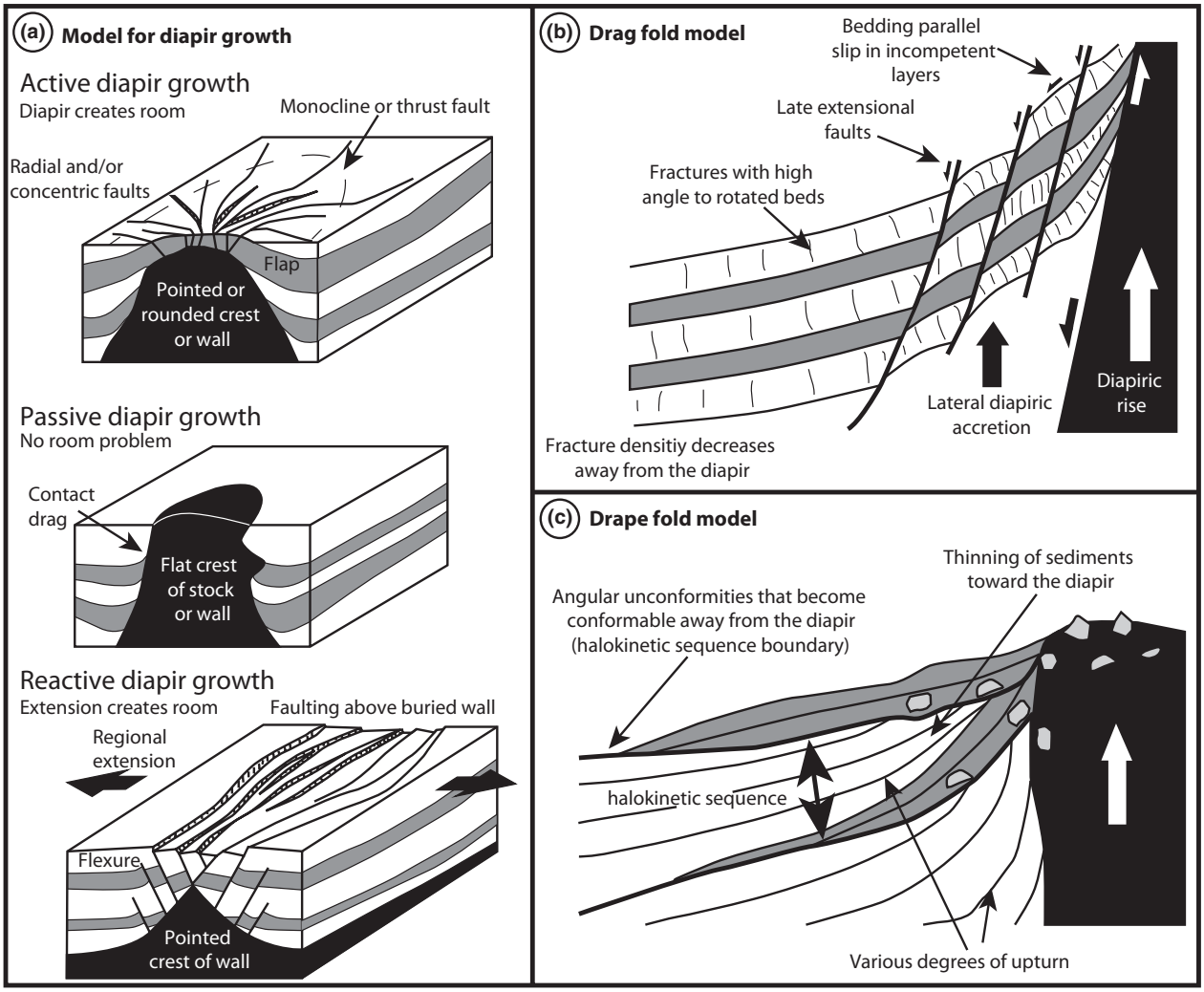

Fig. 1. Models for diapir growth and overburden deformation. (a) Active, passive and reactive diapir growth models (modified from Jackson *et al.*, 1994). (b) Drag fold model (modified from Alsop *et al.*, 2000). (c) Drape fold model (modified from Giles & Lawton, 2002).

thin towards the diapir, major unconformities and upturned strata. The aim here was to describe and discuss the deformation patterns and sedimentary response of strata related to the diapir growth. This aim will be achieved by addressing: (i) how and when did the Bakio diapir rise? (ii) how did diapir growth induce overburden deformation? (iii) Are halokinetic sequence models restricted to the El Papalote diapir or relevant for other diapirs worldwide?

The Bakio diapir provides important outcrop-based data, which is relatively rare in the literature and represents a good analogue for petroleum exploration of diapir flanks where poor seismic imaging makes interpretation difficult. This study improves understanding of the timing of the Bakio diapir growth, and provides insights for the drape fold model. This study also shows the interaction of regional and gravity-driven sedimentation triggered by the diapir within halokinetic sequences, and supports a new method for quantifying the rates of diapir growth.

MODELS FOR DIAPIR FORMATION

This section summarizes models for diapir initiation and growth, and presents the two main models of overburden deformation (drag fold vs. drape) and of halokinetic sequences deposition. The term 'salt diapir' is widely used in the literature to describe all salt structures with discordant contacts with its overburden, regardless of the processes of initiation and growth. The formation of salt structures may be driven by different processes such as extension, differential loading or compression. This work focuses only on diapirs developed within extensional basins.

Diapir initiation and growth

Jackson *et al.* (1994) demonstrated that salt diapirs display discordant contacts with the overburden, showing that diapirs pierce the overburden. As the overburden behaves more as a brittle than viscous medium

(Vendeville & Jackson, 1992; Weijermars *et al.*, 1993), Jackson *et al.* (1994) pointed out the space problem in which salt is able to pierce into a brittle overburden. This problem is solved by three piercement modes: active, passive and reactive diapirism (Fig. 1a). In all cases, the driving mechanism for salt flow, and consequently diapir rise, is the pressure difference between the top of a diapir and its surroundings.

Active diapir growth or piercement (Nelson, 1991) corresponds to intrusion of salt through the overburden (Jackson & Talbot, 1991) and is thought to trigger doming and faulting of the diapir roof (Fig. 1a). Viscous salt may pierce the roof if it is thin enough (Jackson *et al.*, 1994).

Passive diapirism (Jackson *et al.*, 1994), also called downbuilding (Barton, 1933), occurs when salt emerges at surface (Fig. 1a). Deposits accumulate around the diapir and wedge out above the diapir. In this model, the diapir shape is controlled by the balance between the rates of sediment accumulation and diapir rise (Vendeville & Jackson, 1993). When the rates are equal, the diapir grows vertically. When the diapir rises faster than the surrounding sediments deposit, salt may reach the basin floor and spread laterally. By contrast, when sediments aggrade faster than salt rise, sediments onlap and progressively cover the outcropping salt; in this case, the diapir may cease rising because of the sediment load above the diapir.

Reactive diapirism corresponds to diapir salt rising in response to regional tectonics (Fig. 1a). Jackson *et al.* (1994) and Vendeville & Jackson (1992) demonstrated that reactive diapirs develop below extensional half grabens or grabens (Fig. 1a). The balance between faulting and sedimentation may control diapir initiation, as normal faults thin the overburden yet sedimentation increases the thickness of the overburden. Rapid extension with low sedimentation rates leads to progressive thinning of the diapir roof and can evolve towards active and then passive diapir growth. Low extension and high sedimentation rates lead to diapir burial and normal fault growth (Vendeville & Jackson, 1993).

As viscous evaporites cannot pierce through a thick overburden, there are two main ways to initiate diapir growth: either diapirs initiate early when the overburden is thin and unconsolidated or tectonics trigger latter diapir growth by thinning the overburden (Jackson *et al.*, 1994). Hudec *et al.* (2009) and Ings & Beaumont (2010) showed that early compression of a thin overburden may initiate diapir growth. In addition, Jackson *et al.* (1994) demonstrated that regional extension is the most effective process to trigger reactive diapirism when there is a thick overburden. This implies that many diapirs initiated first in response to compression or extension, but subsequently experienced a rapid stage of active diapirism, which permitted piercement of the roof. This allows the diapir to evolve passively. If a diapir is buried by a thick overburden (in the case of a high sedimentation rate), it may prevent further diapir growth (Jackson *et al.*, 1994).

Diapir related deformation

Overburden deformation along diapir flanks has been widely reported in several studies (e.g. Jackson & Talbot, 1991; Jackson *et al.*, 1994; Alsop *et al.*, 1995, 2000; Alsop, 1996; Giles & Lawton, 2002; Rowan *et al.*, 2003). Steep, vertical or overturned strata are widespread, associated with rapid thinning towards the diapir (Alsop *et al.*, 2000). The dip of adjacent strata decrease some distance away from the salt (*ca.* 300–2000 m), depending on the diapir size (Schultz-Ela, 2003). Concentric and/or radial faults also affect diapir flanks (Stewart, 2006).

Two main mechanisms have been proposed to explain overburden deformation induced by salt rise: drag and drape folding (Fig. 1b and c). Drag folds or external shear zones (Jackson & Talbot, 1991; Jackson *et al.*, 1994; Alsop *et al.*, 1995, 2000; Alsop, 1996) involve shearing and deformation of consolidated sediments, along the diapir edges (Fig. 1b). In contrast, drape folds (Schultz-Ela, 2003) are related to deformation of unconsolidated sediments, where folding is explained by differential vertical motion on the diapir edges, between uplift of the diapir roof and subsidence of diapir flanks (Fig. 1c). As the older stata undergo greater tilting than younger strata, this explains various degrees of tilting, unconformities and thinning of deposits towards the diapir. It also explains why slumps may develop on diapir flanks (e.g. Giles & Lawton, 2002; Rowan *et al.*, 2003), as local steepening by drape folding may trigger slumps and other gravity-driven deposits.

Halokinetic sequences

Sedimentary packages bounded by unconformities, with lower gravity-driven deposits and upper fine-grained deposits (Fig. 1c) are described in the overburden of the El Papalote diapir (Giles & Lawton, 2002; Rowan *et al.*, 2003). Giles & Lawton (2002) and Rowan *et al.* (2003) interpreted such stacked packages as the result of cyclic processes. These authors invoked the concept of halokinetic sequences controlled by drape folding. Such sequences are dictated by the balance between the rates of diapir rise and adjacent sedimentation. When diapir rise exceeds sedimentation, the diapir produces positive surface relief and upturned strata. Uplift of the diapir roof may lead to sediment sliding and redeposition; thus gravity-driven deposits may develop unconformably on eroded upturned strata. If uplift and roof destabilization are sufficient, the diapir may breach the basin floor. When sedimentation exceeds the diapir rise, the diapir may be buried. The slope of the flanks is assumed to become gentler due to sediment onlap on the dipping slope. This explains the progressive decrease in gravity-driven deposits in the upper part of the halokinetic sequence. Cycles of salt doming and onlap lead to deposition of stacked halokinetic sequences bounded by angular unconformities. Angular unconformities develop during doming

associated with erosion of upturned strata. Halokinetic sequences represent cycles of passive diapirism and small-scale active diapirism when salt periodically rises and pierces the diapir roof (Rowan *et al.*, 2003).

Giles and Rowan (2012) provided new concepts for halokinetic sequences with two end-member types: the hook and the wedge halokinetic sequences. The hook halokinetic sequences have high-angle unconformities and common gravity-driven deposits with rapid facies variations associated with narrow zones of drape folding. Hook halokinetic sequences are found when diapir rise rate exceeds sedimentation rate. The wedge halokinetic sequences are characterized by low-angle unconformities, less common gravity-driven deposits, gradational facies variations and are associated with broad zone of drape folding. Wedge halokinetic sequences are found where sedimentation rate exceeds diapir rise rate.

GEOLOGICAL SETTING

Mesozoic history of the Basque–Cantabrian Basin

The Bakio diapir belongs to the northern edge of the Basque Trough, in the northern part of the Basque–Cantabrian Basin (Fig. 2), located between the Iberian and European plates. Extension and subsidence in the basin are driven by the opening of the Bay of Biscay and rotation of Iberia during the Cretaceous (García-Mondéjar *et al.*, 1996). The subsidence is governed by major NW–SE-striking faults and minor SW–NE-, N–S- and E–W-striking faults forming a complex pattern with several depocentres (Vicente-Bravo & Robles, 1995; García-Mondéjar *et al.*, 1996) (Fig. 2).

The evolution of this basin may be summarized into three sedimentary stages. The first stage is characterized by limited subsidence and by thin shallow-water siliciclastic and calcareous sediments deposition, from Triassic to Barremian (Rosales *et al.*, 2002). Triassic reds clays and gypsum accumulated during this first stage. The second stage corresponds to Aptian to Middle Albian shallow-water Urgonian limestones and marls deposition in deeper environments (Martín-Chivelet *et al.*, 2002; García-Mondéjar *et al.*, 2004). The last stage is characterized by an important subsidence and by the development of Late Albian to Cenomanian siliciclastic turbidites alternating with lutites. These facies are regionally called the Black Flysch units. Aptian–Albian units are locally 7000 m thick, in the main depocentre, called the Basque Trough. At present, the Basque–Cantabrian Basin corresponds to the westernmost part of the Pyrenean realm (Fig. 2), with limited N–S shortening estimated between 25 km (Gómez *et al.*, 2002) and 40–50 km (Ábalos *et al.*, 2008).

The oldest Mesozoic deposits of the Basque–Cantabrian Basin, composed of Triassic gypsum and red clays crop out in several diapirs. Among these diapirs, the Estella-Lizarra, Salinas de Oro, Gulina, and Mena diapirs (García-Mondéjar *et al.*, 1996), Pondra and Laredo Bay diapirs (López-Horgue *et al.*, 2010) and Gernika diapir (García-Mondéjar & Robador, 1986-1987) were rising during Albian times. Several of these diapirs are located at the intersection between major Hercynian basement faults (García-Mondéjar *et al.*, 1996) (Fig. 2), reactivated during the opening of the Basque–Cantabrian Basin. Basement faulting controlled thin-skinned tectonics and formation of halokinetic structures during Middle–Late Albian times (Bodego & Agirrezabala, 2013). Early Aptian deposits thinning towards the Gernika diapir, located few kilometres eastward from the Bakio diapir, recorded diapir growth during this time (Agirrezabala & García-Mondéjar, 1989). An isolated carbonate platform developed

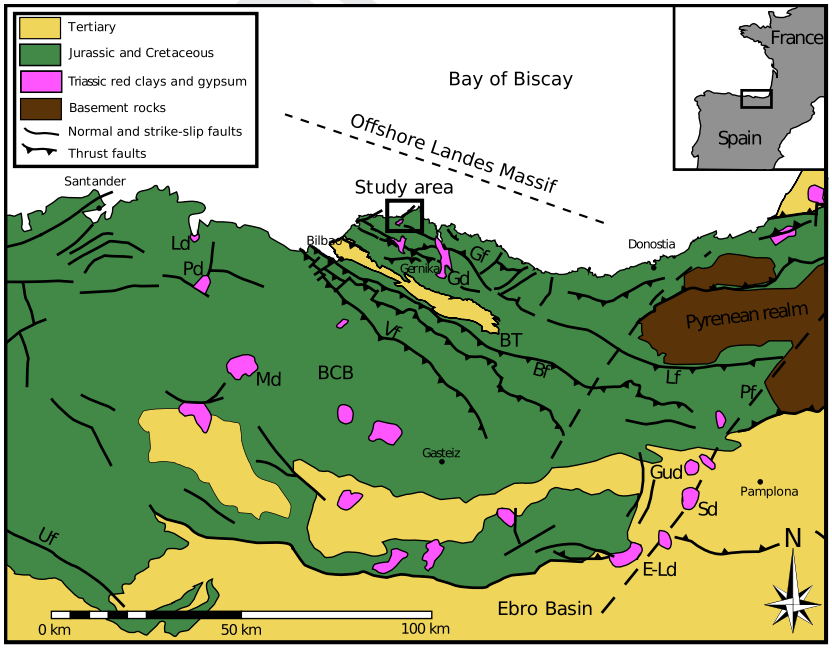

Fig. 2. Geological map of the Basque–Cantabrian Basin (simplified from Ábalos *et al.*, 2008). BCB: Basque–Cantabrian Basin. BT: Basque Trough, Uf: Ubierna fault, Vf: Villaro fault, Bf: Bilbao fault, Gf: Gernika fault, Lf: Leitza fault, Pf: Pamplona fault, Ld: Larredo diapir, Pd: Pondra diapir, Md: Mena diapir, Gd: Gernika diapir, E-Ld: Estella-Lizarra diapir, Sd: Salinas de Oro diapir, Gud: Gulina diapir. The dotted line indicates the possible location of the edge of the Landes Massif, currently offshore.

top of this diapir, associated with slope apron facies deposited at its edge, during Early to Middle Albian times (García-Mondéjar & Robador, 1986-1987). Angular unconformities and lateral facies changes in the Bakio overburden (García-Mondéjar & Robador, 1986-1987; Robles *et al.*, 1988) suggest a similar evolution for both the Bakio and Gernika diapirs. The Bakio diapir is elongated along an NE–SW axis (Fig. 3a); its northernmost part is currently located offshore. The diapir surface trace coincides with the topographical depression where the village of Bakio is located, whereas surrounding relief corresponds to the overburden (Fig. 3b). The diapir is cored by Triassic red clays, gypsum and ophites enclaves (Triassic tholeiitic magmatic rocks), cropping out east of the Bakio beach.

Detailed stratigraphy around the Bakio diapir

Sedimentary rocks of the Bakio overburden include seven stratigraphical units (Fig. 4). In stratigraphical order, the Bakio marls and the Gaztelugatxe units, and the Bakio breccias Fm. correspond to the latest Urgonian deposits of the area. The Sollube, Cabo Matxitxako, Punta de Bakio and Jata units correspond to the first units of the Black Flysch Group.

The Bakio marls unit crops out only in the eastern flank of the Bakio diapir (Fig. 3a). This unit is composed of marls interbedded with thin-bedded packstones, deposited in an outer shelf setting. The Gaztelugatxe unit is found NE of the Bakio diapir, on the Gaztelugatxe and Aketxe islands, and on the mainland coast in front of Aketxe island. García-Mondéjar & Robador (1986-1987) and Robles *et al.* (1988) interpreted this unit as a massive carbonate platform, although several sets of fractures give a brecciated appearance to the limestone and render identification of stratigraphical surfaces difficult. The Bakio breccias Fm. is 550 m thick and is composed of breccias with floatstone blocks, either orthobreccias or parabreccias (with marly matrix), interbedded with marls and

COLOR

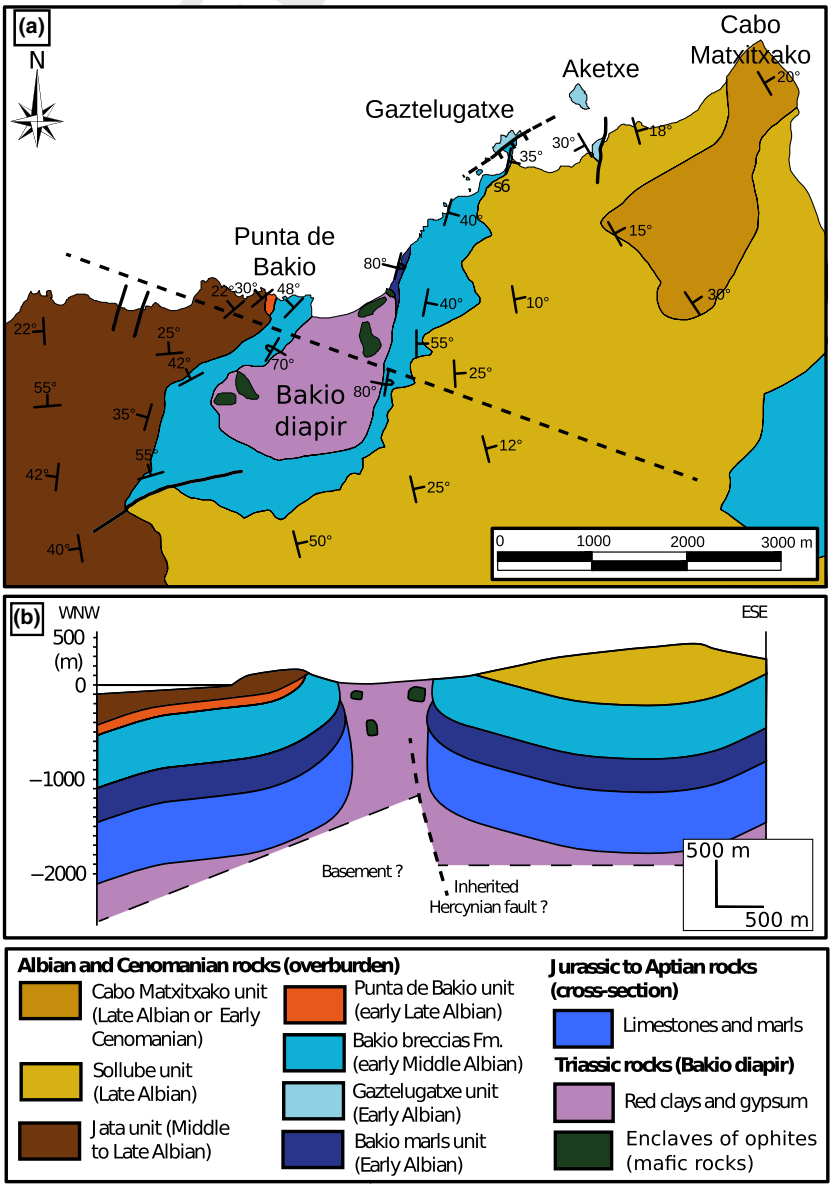

Fig. 3. (a) Geological map of the Bakio area and, (b) cross-section through the Bakio diapir, based on new field work and data from Robles *et al.* (1988b) and Robles *et al.* (1989), García-Mondéjar & Robador (1986-1987), Pujalte *et al.* (1986-1987), Vicente-Bravo & Robles (1991a,b). The dotted line indicates the location of the cross-section.

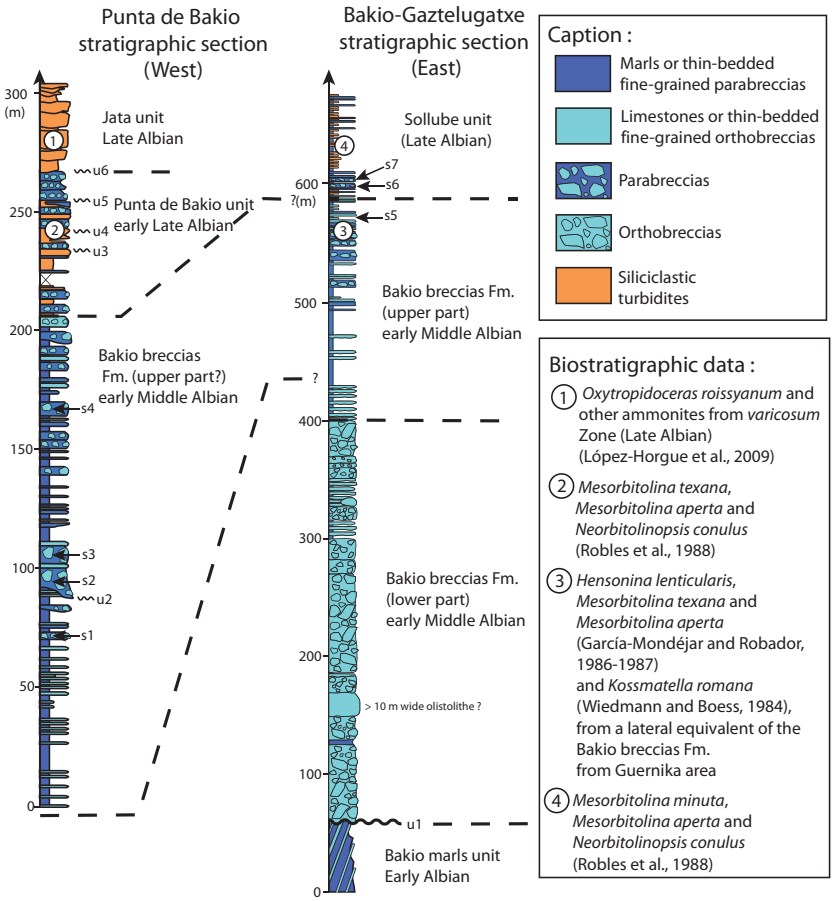

Fig. 4. Stratigraphical sections on the Bakio diapir flanks and their possible correlations based on biostratigraphical data from Wiedmann & Boess (1984), García-Mondéjar & Robador (1986-1987), Robles *et al.* (1988) and López-Horgue *et al.* (2009). The Gaztelugatxe limestones are not represented here. These limestones crop out NE of Bakio, in the footwall of the Gaztelugatxe fault and are probably a lateral equivalent of the Bakio breccias Fm. As the Bakio breccias Fm. to the west has the same facies than the upper part of the Bakio breccias Fm. to the east, both part are probably lateral equivalent. The Punta de Bakio and the Jata units are probably the lateral equivalent of the Sollube unit. Unconformities are labelled from u1 to u6 and slumped intervals from s1 to s7, depending on their stratigraphical location.

thin-bedded grainstones. Breccias, interpreted as slope apron facies, are associated with olistolithes up to 1 m wide. The eastern flank of the diapir displays a thick accumulation of orthobreccias (*ca.* 350 m) in the lower part of the Bakio breccias Fm., and alternating parabreccias and marls in the upper part (200 m thick, Fig. 4). The western flank shows parabreccias and thin-bedded orthobreccias interbedded with marls that correspond to a lateral equivalent of the upper part in the eastern flank (Fig. 4). For García-Mondéjar & Robador (1986-1987) and Robles *et al.* (1988), the Gaztelugatxe unit, representing the southern part of a carbonate platform located farther north, currently offshore, is the source for breccias in the eastern flank of the diapir.

The Sollube unit mainly consists of thin-bedded, fine-grained siliciclastic turbidites interbedded with marls. The Cabo Matxitxako unit is composed of amalgamated thick-bedded coarse-grained siliciclastic turbidites. The Sollube and Cabo Matxitxako units are found in the eastern flank of the Bakio diapir (Fig. 3a). West of the diapir, the Punta de Bakio unit consists of marls interbedded with thin-bedded, fine-grained siliciclastic turbidites, beds of parabreccias with limestone blocks, quartz pebbles and reworked turbidites. The Jata unit is composed of marls alternating with fine-grained to coarse-grained siliciclastic turbidites and include slumps and breccias. The Punta de Bakio and Jata units are found only in the western flank of the Bakio diapir (Fig. 4). The Landes Massif, currently located offshore, is considered as the source for the siliciclastic units (Voort, 1963; Rat, 1988; Robles *et al.*, 1988; Agirrezabala, 1996; García-Mondéjar *et al.*, 1996; Martín-Chivelet *et al.*, 2002).

Sparse biostratigraphical data and important lateral facies variations in the Bakio area make correlations between units from either flanks of the diapir difficult. The available biostratigraphical data (Wiedmann & Boess, 1984; García-Mondéjar & Robador, 1986-1987; Robles *et al.*, 1988; López-Horgue *et al.*, 2009) are summarized in Fig. 4. According to these data, the Urgonian units are Early to Middle Albian in age. The Bakio breccias Fm. is early Middle Albian in age (*dentatus* Zone). The Bakio marls and the Gaztelugatxe units are not directly dated. The Bakio marls unit is probably Early Albian in age, as the Bakio breccias Fm. overlies it. The Gaztelugatxe unit may be Early Albian to early Middle Albian in age as this unit is assumed to be the source for the Bakio breccias Fm.

The units of the Black Flysch Group are Middle to Late Albian in age. The Punta de Bakio unit and the Sollube unit are early Late Albian and Late Albian in age respectively. The Jata unit (Middle to Late Albian) has been dated as early Middle Albian (*dentatus* Zone) by López-Horgue *et al.* (2009) further west, whereas it overlies the Punta de Bakio unit (early Late Albian) in the western flank of the Bakio diapir. The Sollube unit is probably a lateral equivalent of the Punta de Bakio and

Jata units. The Cabo Matxitxako unit is not dated and may be Late Albian or Early Cenomanian in age.

The latest Urgonian unit (Bakio breccias Fm.) is early Middle Albian in age whereas overlying units of the Black Flysch Group are Late Albian in age. This defines a hiatus of most of the Middle Albian, as described by García-Mondéjar *et al.* (2004) and López-Horgue *et al.* (2009).

METHODS

This work used field data as bedding planes, slumps axes, fault orientations measurement, stratigraphical sections building and facies analyses. Some of these methods need special explanations that are presented below.

Restoration of sedimentary structures

In this study, sea floor dip direction was inferred using several sedimentary structures. Sole marks in turbidites provided directions of turbidity flows and slumping directions may be deduced as they may be roughly perpendicular to the mean trend of slump fold axes (e.g. Alsop & Marco, 2011). Because diapir growth tilted most of beds in the overburden, a restoration was necessary. All beds with sedimentary structures have been tilted back to a horizontal position because gravitational processes occur on low-angle slopes, as little as few degrees (not higher than 10° in submarine environment). This assumption of initially horizontal bed is suitable for turbidites as such deposits develop on low-angle slopes (<1°). Slumps may deposit on steeper slopes, not higher than 10°. However, an error of *ca.* 10° in the dip of the initial slope may not modify the mean trend of slump folds axes significantly, thus may not change the associated slumping direction. Therefore, the assumption of initially horizontal bed is also suitable for these deposits, but less accurate compared with turbidites.

The TrackDip method

TrackDip is a method initially developed by Basile *et al.* (2009) to analyse vertical variations of bedding attitude from borehole data or from stratigraphical sections with strike and dip measures. TrackDip divides the data set from the borehole or stratigraphical section into different intervals with a given thickness, each interval is called a window. Successive windows from large to small scales are created by dividing the entire section first into two windows (largest window scale), then into three windows and this procedure continues until it reaches the smallest window scale (thinnest interval including at least one bedding attitude measurement). For each window, a mean plane is calculated from bedding plane data included in the window. The mean planes may not have a geological meaning, but allow comparison with neighbouring windows (windows above and below a given window). When two adjacent windows display different mean planes, the tilt between these planes is calculated, by reference to the upper window. These tilts are defined by a tilt axis, a tilt angle and a dip direction. The TrackDip results are shown in a graph with window size on *X*-axis and thickness of the entire section on *Y*-axis. If similar tilts (similar trend axis, angle and dip direction) are found at different scales, TrackDip is able to detect and follow these tilts from large to small windows, for the same depth intervals (Figs S1 and S2). Tilts detected from large to small windows are represented in the graph by lines connecting similar tilts found at different scales. Tilts are considered as significant if they can be tracked at least for three successive scales, with significant tilt angles (>4°), and if axis trend variations do not exceed 30° (Basile *et al.*, 2009).

In case of a sudden change in bedding attitude, the tilt may be detected from large to small windows, with the highest tilt angle found at the smallest windows, because the change is local. For example, the highest tilt angle is expected between the smallest windows below and above an angular unconformity. On the contrary, the largest windows may include other tilts considered as noise and thus a lower angle is expected. In case of gradual change in bedding attitude, the tilt between large windows may represent the entire gradual tilt, and thus the tilt angle is expected to correspond to the highest tilt angle. By contrast, the tilt between small windows represents only one increment of tilting, and thus the tilt angle is expected to be lower. More details for the TrackDip method are given in Basile *et al.* (2009).

Calculation of the uplift rates of the diapir roof

The amplitude of diapir roof uplift may be estimated using tilt angles within synkinematic strata related to diapir growth. If biostratigraphical data are available within the synkinematic strata, it is possible to give the associated uplift rates of the diapir crest.

Considering a very simple model for flank tilting related to differential displacement between the diapir axis and its sides (Fig. 5), the uplift of the roof may be roughly estimated following equation 1:

$$Us = Ww \times \tan \alpha \quad (1)$$

where

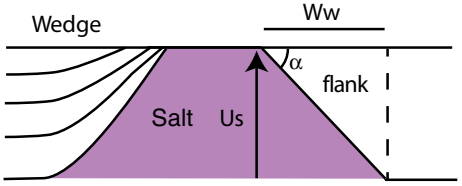

Fig. 5. Simple model of salt rise used to estimate salt height from the dip angle along the flanks, where Us is the height of salt after diapir growth (or differential vertical displacement), α the tilt angle in the wedge and Ww the width of the wedge.

COLOR

Us is the uplift of salt after diapir growth (or differential vertical displacement), α the tilt angle in the wedge and Ww the width of the wedge.

Measurement of the tilt angles has to be made where angles are higher (near the salt) because dip angles of upturned strata vary laterally and vertically within the overburden.

This simple equation may be valid only if the diapir is buried, as each increment of salt rising may trigger flanks tilting (Fig. 5). Therefore, uplift rate of the roof and salt flow velocity may be approximately equal, if convective motions within salt are neglected. If salt reaches the surface, salt may flow without tilting the adjacent wedges, thus salt flow velocity may exceed uplift rate of the diapir edge. In this case, this equation may give underestimated results.

STRUCTURES IN THE DIAPIR FLANKS

Sedimentary wedges and unconformities

The western part of the Bakio bay (Punta de Bakio cliffs) displays a well-exposed wedge-shaped structure (Fig. 6a), adjacent to the salt diapir. From east to west, this wedge is composed of the Bakio Breccias Fm., Punta de Bakio and Jata units (Fig. 6b). The Punta de Bakio unit displays several angular unconformities, including its top (Fig. 6b). All units thin eastward and their bedding dips decrease westward. Strata are dipping from 80° towards the SE (overturned strata) in the basal part the Bakio Breccias Fm., to 20° towards the NW in the uppermost part of the Punta de Bakio unit. In the Bakio breccias Fm., four parabreccia beds (s1 to s4) contain slumped clasts with associated folds (Fig. 4). About 700 m away from the diapir, the Jata unit is horizontal on the coastline. To the SW, the Jata unit unconformably overlies the Bakio breccias Fm., showing that the wedge extends towards the SW. Here, the Punta de Bakio unit is absent because it pinches out towards the diapir.

Another wedge crops out along the eastern diapir flank. In the lower part of the wedge, the Bakio breccias Fm. unconformably overlies the overturned Bakio marls unit (unconformity u1 in Fig. 4). The angular unconformity indicates an important tilt of the eastern flank, which occurred before deposition of the Bakio breccias Fm. In the upper part of the wedge, the Bakio breccias Fm. and the Sollube unit display a progressive decrease in their bedding dips, from 60° to 20° towards the SE. To the south, the Sollube unit unconformably overlies the Bakio breccias Fm., showing that this wedge also extends southward.

The Gaztelugatxe normal fault

A vertical and irregular fault surface, with an apparent vertical offset (Fig. 7a and b), roughly striking NE–SW at

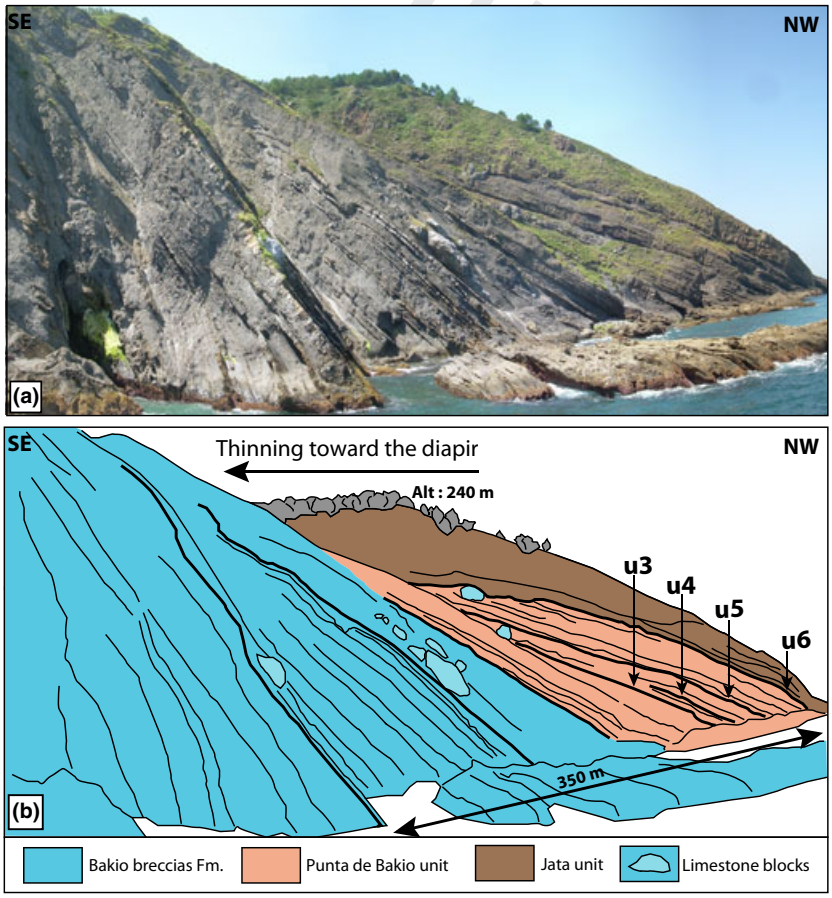

Fig. 6. (a) Westward view of the Punta de Bakio sedimentary wedge. (b) Interpretation of the wedge, composed from bottom to top of the Bakio breccias Fm., Punta de Bakio and Jata units. These units exhibit a westward decreasing dip and the Punta de Bakio unit displays four angular unconformities (u3 to u6, Fig. 5). Near the diapir contact, beds are overturned (about 10 m to the east of the picture).

COLOR

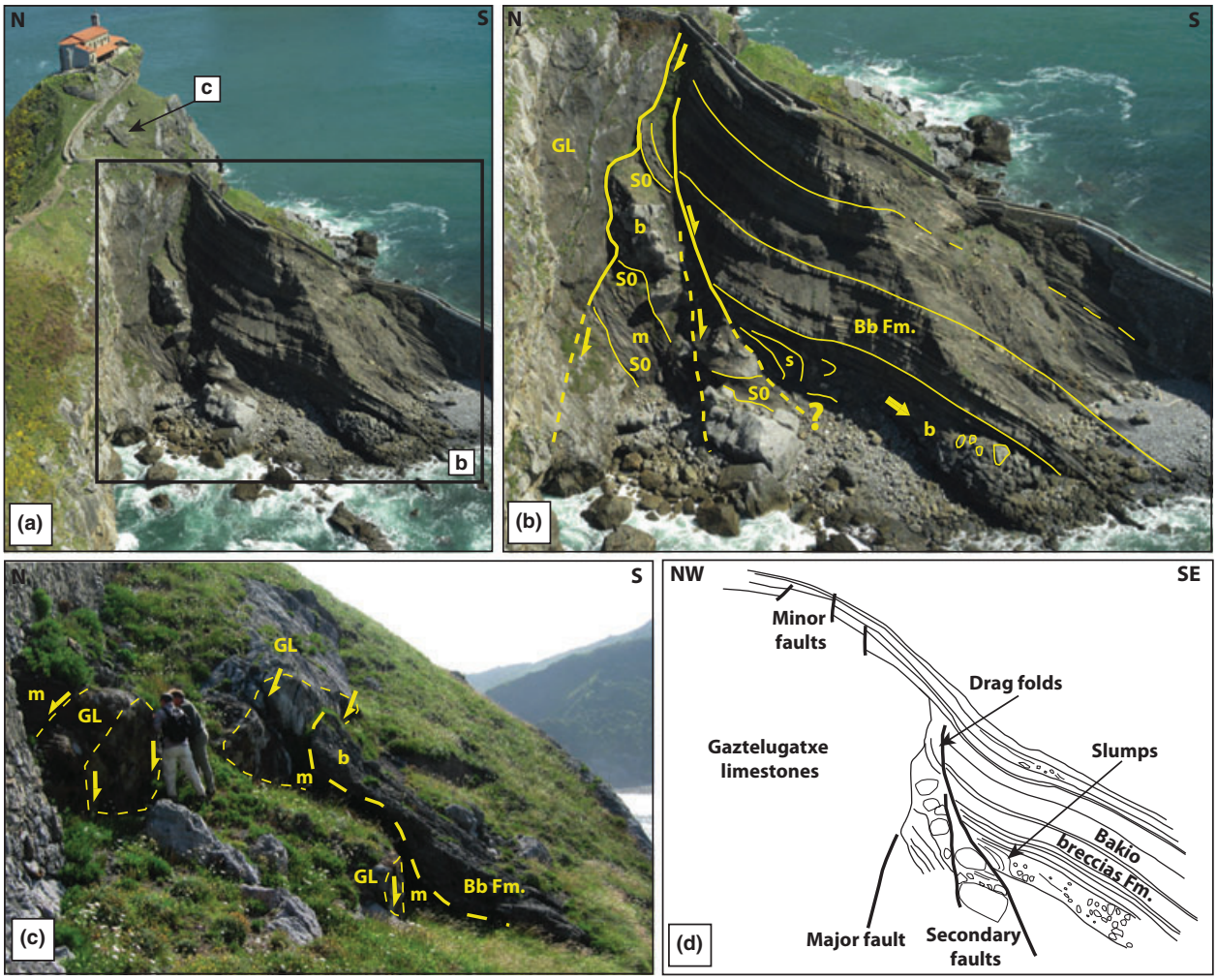

Fig. 7. (a) Aerial view of Gaztelugatxe fault from the SW, with the Gaztelugatxe unit to the NW (footwall) and the upper part of the Bakio breccias Fm. to the SE (hanging wall). (b) Detail of the aerial view of the Gaztelugatxe fault from the SW illustrating the irregular fault scarp developed in the Gaztelugatxe unit (GL) and two secondary faults developed in the upper part of the Bakio breccias Fm. (Bb Fm.). S0: bedding planes, m: marls, b: breccias, s: slumps. (c) View of minor faults top of the footwall, offsetting the Gaztelugatxe unit (GL). Marls (m) and breccias (b) of the upper part of the Bakio breccias Fm. (Bb Fm.) cover the southernmost fault. Slickensides developed on these faults planes. After tilting to synsedimentary orientation by rotating bedding planes covering the faults, these slickensides give a normal offset (Fig. 4e). (d) Interpretation of the entire outcrop.

present (N048°, 90°) is located on the Gaztelugatxe Island (Fig. 3a), about 1 km NE of Bakio. The footwall, located NW, is composed of the Gaztelugatxe limestones (Fig. 7a and b). The hanging wall, located SE, is composed of the upper part of the Bakio breccias Fm. (Fig. 7a and b). Although, data are lacking north of the present day coastline, mapping suggests that the Bakio breccias Fm. only develops south of this fault. This suggests that this unit pinches out northward and onlap on the Gaztelugatxe fault scarp.

In the hanging wall, the most tilted beds are located adjacent to the major fault scarp and are slightly drag folded showing a normal displacement (Fig. 7b). Two minor normal faults, roughly parallel to the major fault scarp, offset the upper part of the Bakio breccias Fm. (Fig. 7b and d). These faults are synsedimentary faults as their offsets decrease upward and as they are buried by the uppermost part of the Bakio breccias Fm. (Fig. 7d). SE of these faults, three slumped intervals are located at the top of the Bakio breccias Fm. (s5 slumps, Fig. 4) and in the basal part of the Sollube unit (s6 and s7 slumps, Fig. 4). Below these slumps, another slumped bed passes laterally into parabreccias (Fig. 7b and d).

In the footwall, three other secondary normal faults, locally covered by a ferruginous crust, offset the Gaztelugatxe limestones (Fig. 7c). On these minor fault scarps, slickensides give an apparent right-lateral strike-slip displacement with a normal component. Similarly to the major fault, the uppermost part of the Bakio breccias Fm. buried these minor faults (Fig. 7d).

Minor faults in the Bakio overburden

Several faults (length of fault traces from metre to decametre scale) crop out in the Bakio overburden. The fault network presents three preferential strikes (N030°, N110°

and N160°). These faults similarly affect beds, whatever their degree of tilting (from overturned beds to horizontal beds), suggesting that faulting occurred after flank tilting. Moreover, there is neither evidence for lateral facies nor thickness changes, nor associated gravity-driven deposits. This shows that these faults affected beds after their deposition. Similar fault sets affect the whole Albian sedimentary succession, both east (Matxitxako Cape, located *ca.* 4 km east of the Bakio diapir) and west of Bakio (from Bakio to Armintza). This means that they are not related to the diapir growth, but to regional deformation postdating the diapir growth.

STRUCTURAL ANALYSES AND IMPACT OF DIAPIR GROWTH ON SEDIMENTATION

This section offers a structural interpretation for the major outcrops described in the previous section. In addition, sedimentological data from two stratigraphical sections studied on either flank of the diapir are discussed.

Interpretation of the sedimentary wedges and unconformities

Stereographical plots of bedding planes from the western wedge (Fig. 8c and d) give the tilt axis orientation responsible of bedding dip variations in the wedge (Fig. 6). It indicates a progressive tilt with a horizontal axis striking N067°, in the coastline (Fig. 8c) and an axis striking N042° dipping 19°NE, in the second outcrop (Fig. 8d), to the south.

Stereographical plots of bedding planes from the eastern wedge (Fig. 8f and g) show a progressive tilt with an axis striking N009° dipping 03°NE in the coastline (Fig. 8f) and an axis striking N021° dipping 9°N, in the second outcrop (Fig. 8g), to the south.

The map trace of the diapir, with the western and eastern flanks striking NE–SW and N–S, respectively, suggests northward convergence of the flanks (Fig. 8a). Tilting axes calculated from bedding planes in wedges are parallel to the flanks and to the mean diapir axis (Fig. 8b). This demonstrates the creation of wedges and angular unconformities by flanks tilting (u1 to u5, Fig. 4) during diapir growth. Therefore, the Bakio breccias Fm., Sollube and Punta de Bakio units and the base of the Jata unit were deposited during diapir growth.

Interpretation of Gaztelugatxe normal fault

The Gaztelugatxe outcrop has been interpreted as a synsedimentary normal fault scarp (García-Mondéjar & Robador, 1986-1987; Robles *et al.*, 1988). The irregular aspect of the fault scarp suggests submarine erosion of the scarp (García-Mondéjar & Robador, 1986-1987; Robles *et al.*, 1988). Fault motion occurred during deposition of the Bakio breccias Fm., as the fault is covered by the uppermost part of this unit (Fig. 7d). This supports the geometry of the Bakio breccias Fm. that seems to pinch out northward on the fault scarp. This implies uplift in the footwall and deposition of the Bakio breccias Fm. in the hanging wall occurring at the same time. Limestones blocks in breccias and the Gatelugatxe limestones from the footwall exhibit similar facies, thus the Gatelugatxe limestones were the source for breccias, as proposed by García-Mondéjar & Robador (1986-1987). The thick slumped bed changing laterally into parabreccias in the hanging wall (Fig. 7b) reveals downslope flow transformation towards the SE, consistent with a source from the north, from the Gaztelugatxe limestones.

Reworking related to tectonics, probably from the Gaztelugatxe fault scarp is demonstrated by the size and abundance of olistolithes, up to 1 m thick, in the Bakio breccias Fm. Orthobreccias with thick olistolithes in the lower part of the Bakio breccias Fm. implies an episode of intense fault activity. On the contrary, thick marly intervals without olistolithes in the upper part of this unit indicate a decrease in fault activity. The onlap of the uppermost part of the Bakio breccias Fm. that buried the fault and the absence of olitolithes in the overlying Sollube unit confirm the decrease in the fault offset.

The entire structure underwent a late tilting towards the SE (*ca.* 35° along an axis trending N025°) as beds covering the fault are tilted (Fig. 7d). This tilt may be related to Pyrenean shortening. In order to obtain the orientation of structures during Albian times, the uppermost beds of the structure may be back tilted to horizontal (Fig. 8e). After back tilting of these beds, the three small faults and their slickensides (with an apparent right-lateral strike-slip displacement, prior to back-titling) found top of the footwall display a normal displacement (Fig. 8e) consistent with the entire structure.

The Bakio diapir and the major Gaztelugatxe fault are aligned together and share comparable trends, respectively N034° and N048° (Fig. 8a, b and e). The hanging wall of the Gaztelugatxe fault coincides laterally with the subsiding part of the eastern diapir flank, yet the footwall and the uplifting apex of the diapir may be connected. The Bakio breccias Fm. wedges out towards both the Gaztelugatxe fault and the diapir. This points out that both structures activated at the same time and were connected. Consequently, the diapir probably extends offshore, below the footwall of Gaztelugatxe fault.

Slumps triggered by the diapir flanks tilting

Numerous slumped intervals can be observed on both sides of the Bakio diapir, in the Punta de Bakio outcrop (western flank) as at Gaztelugatxe (eastern flank).

Measurements of bedding planes attitudes in each slumped interval in the western flank (s1 to s4) have been made to define the slump fold axes. Restored fold axes

COLOR

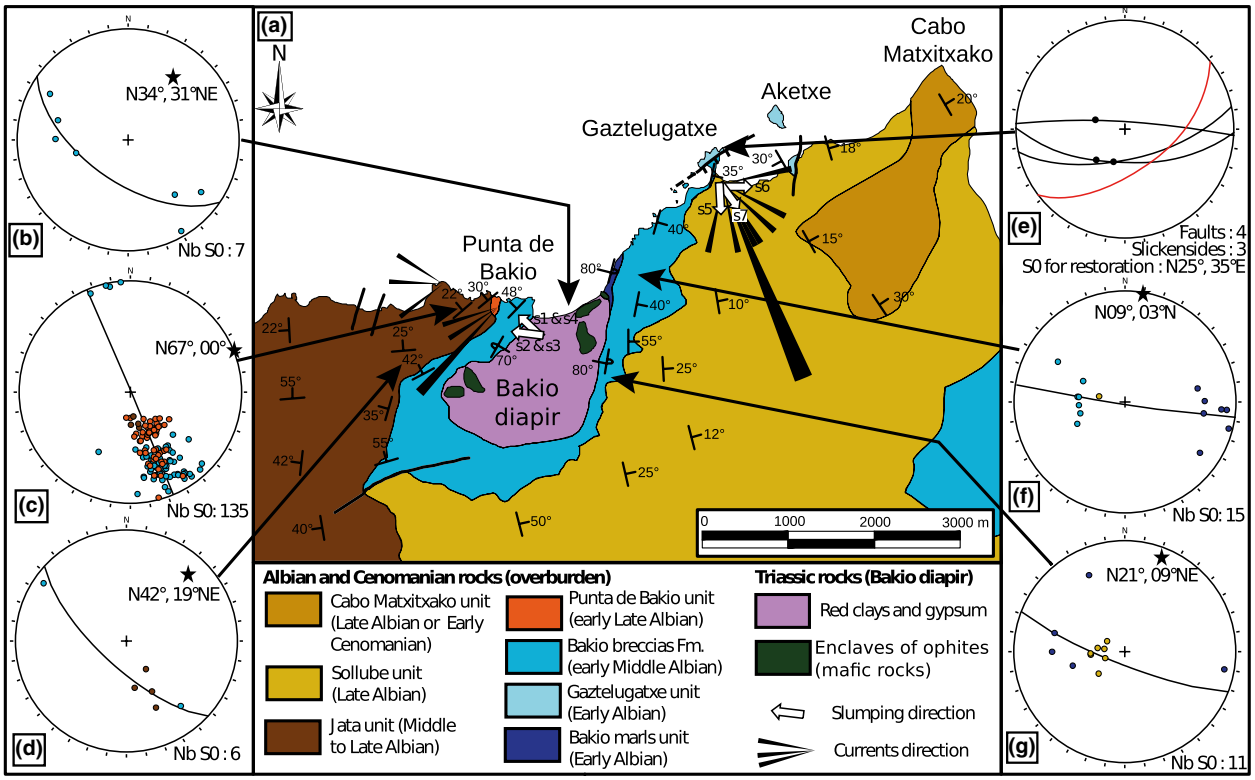

Fig. 8. (a) Geological map of the Bakio area. Black rose diagrams correspond to turbidites currents directions (20 measurements in the Monte Sollube unit, east of Bakio; 8 and 6 measurements in the Punta de Bakio and Jata units, respectively, west of Bakio; short classes include 2 measurements and longer classes include 6 measurements) and white arrows correspond to sliding directions of the s1 to s7 slumps. (b, c, d, f, g) Stereographical plots (lower hemisphere equal-area stereonet) of the mean axis of the diapir (b.) and of the tilt axes (stars) calculated from bedding planes orientations (points, same colours as in map caption) within the wedges along both flanks (c, d, f, g, h). (e) Stereographical plot (lower hemisphere equal-area stereonet) showing the Gaztelugatxe major fault (red plane) and the minor faults top of the footwall of the Gaztelugatxe fault and their slickensides (black planes and circles) restored to synsedimentary orientation by tilting bedding planes covering the faults, to horizontal.

from the four intervals have similar N–S to NW–SE orientations (Fig. 9a–d).

In the hanging wall of the Gaztelugatxe fault, direct measurements of slump fold axes have been made. After restoration to horizontal bedding, slump axes trend preferentially E–W in the s5 interval (Fig. 9e) and roughly NE–SW in the s7 slumped interval (Fig. 9f). In the s6 slumped interval, restored slump axes preferentially trend N160° to N180°, with important dispersal of fold hinges (Fig. 9g and h). Such dispersal of fold hinges is linked to the small length and incurved shape of slump folds, with fold terminations almost perpendicular to the central part (Fig. 9i). Measurements of axial planes have been added to provide more information for slumps movements (Fig. 9g), as in Alsop & Marco (2011). Axial planes also show an important dispersal but with a preferential plan striking N027°, 25°NW, indicating eastward verging folds. Some asymmetric slumps indicate an eastward displacement on an eastward-dipping slope.

In the Punta de Bakio section, the restored fold axes with N–S to NW–SE orientations for the four intervals (Fig. 9a–d) parallel the diapir axis (Fig. 4b). Thus, they are interpreted as resulting from destabilization of sediments during flank tilting and sliding towards the west or the NW.

In the hanging wall of the Gaztelugatxe fault, slump axes orientations of the s5 interval suggest a southward-dipping slope, whereas the s6 and s7 interval indicate an eastward and a south-eastward-dipping slopes respectively. This points out changes in orientation of the slope through times. Uplift of the footwall of the Gaztelugatxe fault may produce a southward-dipping slope associated with the s5 interval. As the fault became inactive during deposition of the Monte Sollube unit, other processes may explain the s6 and s7 slumped intervals. Diapir flank tilting may create eastward and south-eastward-dipping slope producing the s6 and s7 slumped intervals. Uplift to the north may have lasted throughout Late Albian due to diapir growth, even if the fault became inactive. Sediment destabilization from the edge of the Landes Massif to the north may also explain the s7 slumped interval.

Slump with limestones blocks emanating from the overburden roof in both flanks attest that the source area for gravity-driven deposits including parabreccias is the diapir roof. This implies the development of a carbonate platform also on top of the Bakio diapir, probably due to shallowing and creation of topographical high on the sea floor.

Paleocurrent directions were measured in sole marks of turbidite beds intercalated with slumps and breccias

COLOR

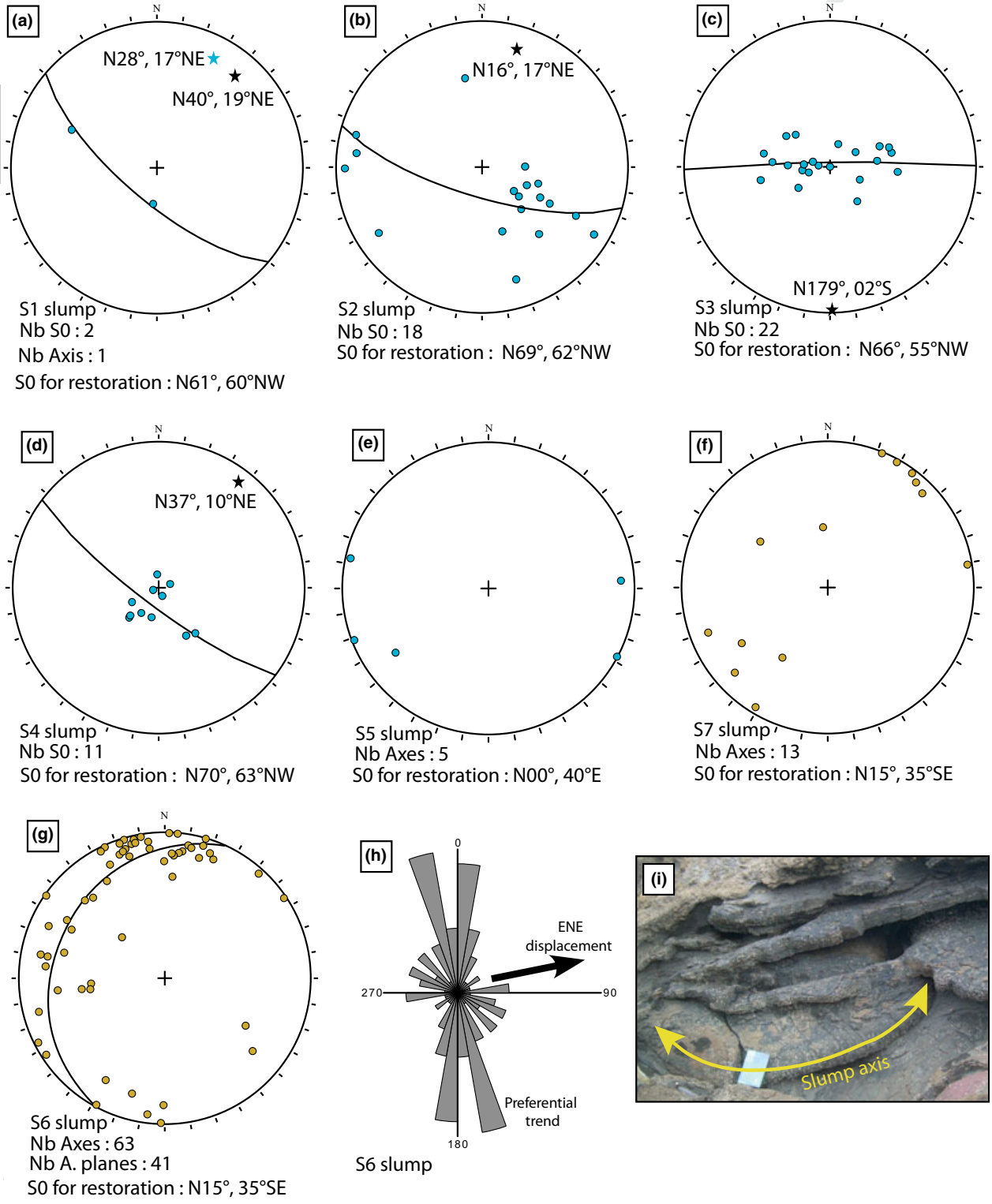

Fig. 9. Stereographical plots (lower hemisphere equal-area stereonet) of bedding planes (s1 to s4) and of slumps axes (s5 to s7) within the s1 to s7 slumped intervals from the Punta de Bakio and the Bakio–Gaztelugatxe stratigraphical section (Fig. 5). (a–d) Bedding planes within the s1 to s4 slumped intervals, black stars correspond to the pole of the great circles calculated from bedding planes orientations and indicate slumps axes. For the s1 fold axis, the blue star corresponds to fold axis, directly measured on the outcrop. (e–g) Slumps folds axes directly measured on the outcrop for the s5 to s7 slumped intervals. For the s6 slumped interval, the best plan calculated from 41 measurements of axial planes has been added. Each plot of bedding planes is restored to synsedimentary orientation by tilting each data set with overlying bedding planes to horizontal. The number of data and S0 used for restoration to horizontal is indicating below each plot. (h) Rose diagram of restored folds axis within the s6 interval. The preferential trend, striking N–S is consistent with a displacement towards ENE. i. Bended slump hinge of the s6 slumped interval.

around the Bakio diapir (in the Sollube, Punta de Bakio and Jata units). Turbidites of the Punta de Bakio unit flowed roughly parallel to the western flank (Fig. 8a). This suggests that the diapir diverted turbidity flows originated from the northern Landes Massif. In the Gaztelugatxe Island, turbidites of the Sollube unit roughly proceeded from the north, with an important dispersion (Fig. 8a). This suggests that turbidity flows emanating from the Landes Massif flowed southward without being influenced by surface relief. The absence of relief at the sea floor confirms that the Gaztelugatxe fault was buried during deposition of the Sollube unit.

Turbidites around the Bakio diapir are interbedded with slumps and parabreccias with limestones blocks, derived from the diapir roof. It implies a multi-source system with turbidity flows emanating from the Landes Massif and breccias with limestones blocks coming from the diapir roof.

Tilts in the Punta de Bakio wedge using the TrackDip method

The TrackDip method (see 4.2 for details of this method) has been used for the Punta de Bakio stratigraphical section, after a systematic measurement of bedding planes attitudes and position (Fig. S1). It represents 135 bedding measurements in a 277 m thick section. The tilts are referenced by a number attributed during TrackDip processing. As all beds are tilted towards the NW due to wedge tilting, arrows pointing towards the NW indicate steeper beds in the lower windows. By contrast, arrows pointing towards the SE indicate steeper beds in the upper windows. This method enables the detection of significant geological structures within the studied section, including unconformities and slumps. Only the tilts with geological significance are presented in Tables S1–S4.

The tilt no. 1 (Table S1) represents a gradual tilt over the whole studied section, as it shows higher tilts between large windows (see 4.2 for methods details). The tilt axis trends N058°, comparable to the axis previously calculated for the entire wedge (N067°, Fig. 8c). Both northwestward tilt direction and axis orientation are consistent with diapir flank tilting. Therefore, this gradual tilt is interpreted as the main tilt that created the sedimentary wedge.

The tilts no. 2–5 represent sudden tilts as the maximal tilt angles are found for the smaller window sizes (Table S1). Tilts no. 2 and 4 enable to detect the unconformities u4 and u2, respectively. Tilts no. 3 and 5 may also be related to an unconformity undetected on the field. The tilts no. 1–5 have similar rotation axis trend and rotation direction, with the exception of tilt no. 4. Therefore, the progressive tilt observed for the whole wedge may be interpreted as the addition of several localized tilts (e.g. tilts no. 2–5). Tilt no. 4 has an opposite rotation direction, comparatively to the tilts no. 1, 2, 3 and 5 (Fig. S1). Such tilt towards the SE indicates steeper beds in the upper windows. As the tilt no. 4 coincides with the base of the s2 slumps, slumps may explain why beds are steeper in the upper windows.

Tilts found at smaller scales display more variations on tilt axis trends. Many changes of orientations are associated with slumped intervals (Fig. S2). In each intervals, tilts axes and measured folded slumps axes are similar. For example, in the s2 slumped interval, tilts (tilts no. 10, 24, 25, 34, 38, 44 and 47, Table S2) and slumps (axis trending N016°, Fig. 9b) share similar axes roughly trending NE–SW (Fig. S2a). In the s3 slumped interval, tilts (tilts no. 22, 23, 41, 42, 43 and 46, Table S3) trend N–S (Fig. S2a), like the N179° fold axis (Fig. 9c). The change in orientation of tilt axis trends also correlates well with the s2–s3 boundary (Fig. S2a). It may correspond to different fold orientations within the s2 and s3 slumped intervals.

At the smallest window sizes (≤10 m), several tilts can be associated as pairs showing opposing dip directions (no. 11 and 18, no. 16 and 30, no. 19 and 29 and no. 20 and 32, Table S4), mostly in slumped structures. For example, the no. 11–18 pair displays similar axes (trending N075° and N065°, respectively) with opposing dip directions (Fig. S2b). Opposing dip directions indicate the presence of steeper beds in the interval comprised between these tilts compared to both the upper and lower intervals, because it is related to slumped structures and not directly to diapir flank tilting. These tilts coincide with the s4 slumped interval (Fig. S2b) and have a trend similar to the fold axis of slumps (N037°, Fig. 9d). This is also the case for the no. 16–30 pair (trending N098° and N068°, respectively), which fit on the s1 slumped interval (Fig. S2c). Similar interpretations may explain the pairs of tilts no. 19 and 29 and no. 20 and 32 as both pairs coincide with slumped beds or breccia beds (Fig. S2c).

Halokinetic sequences

According to Giles & Lawton (2002) and Rowan *et al.* (2003), angular unconformities in diapir flanks may be interpreted as boundaries of halokinetic sequences. A halokinetic sequence corresponds to a set of strata, locally bounded by unconformities, with gravity-driven deposits in the lower part, and fine-grained deposits in the upper part (Fig. 1c).

In the upper part of the Punta de Bakio stratigraphical section, a 3-m thick bed of parabreccia is overlain by siliciclastic turbidites (235–244 m, Fig. 10). This package is bounded by the u4 and u5 unconformity and thus may be interpreted as a halokinetic sequence (Fig. 10). Parabreccias may result from doming in the diapir crest, which creates an unstable slope failing periodically (when diapir rising >accumulation rate), while turbidites onlap the diapir (when diapir rising <accumulation rate). Parabreccias are interpreted as relatively proximal slope apron facies as they exhibit large floatstone blocks (up to 1 m wide) with basal scours, and are often non-graded or inversely

COLOR

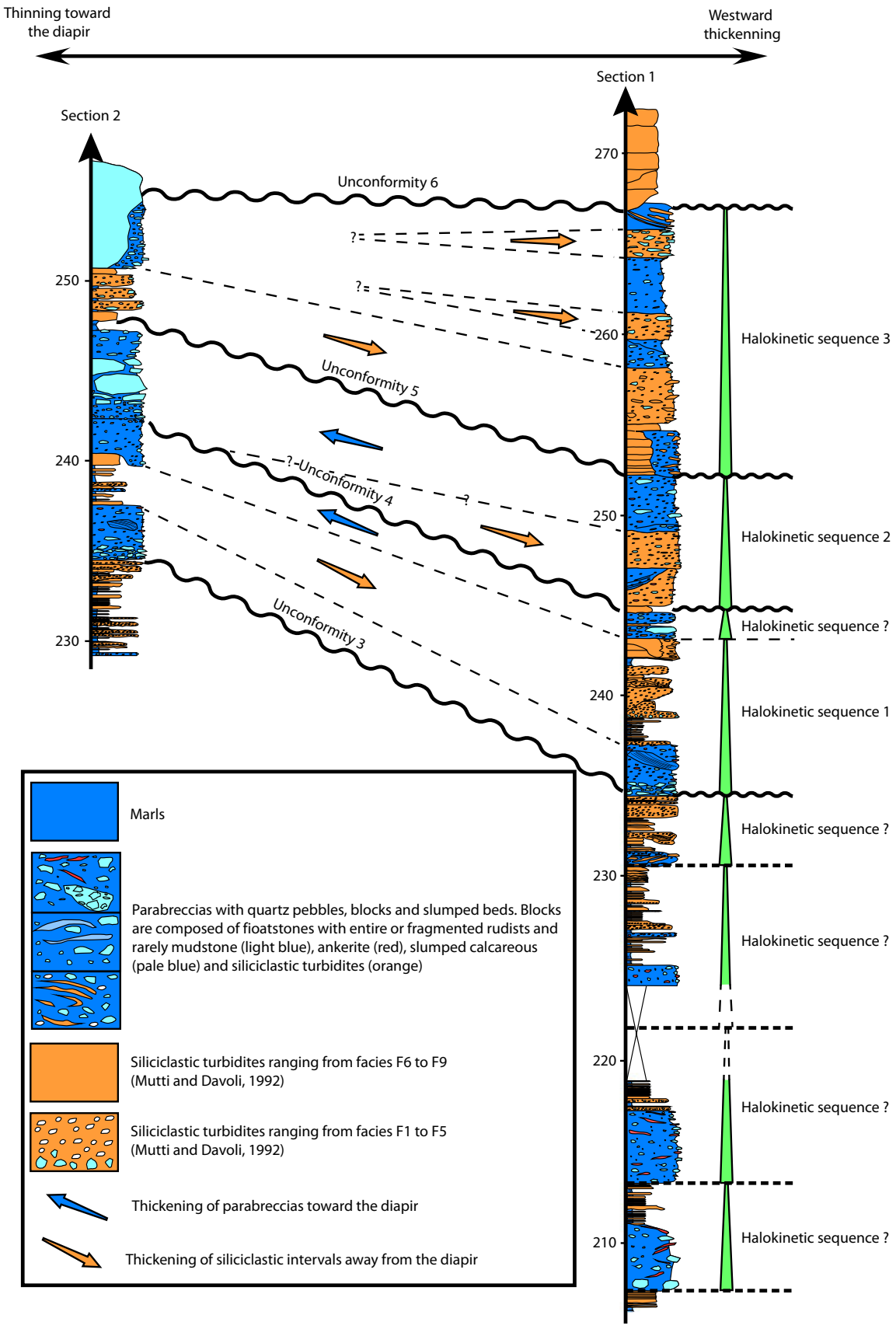

Fig. 10. Top of the Punta de Bakio stratigraphical section illustrating lateral variations, with thinning towards the diapir and angular unconformities (u to u5, Fig. 5). Below the u3 unconformity, the cyclic patterns of sedimentary packages with parabreccias in the lower part and with turbidites in the upper part suggest that other halokinetic sequences may be present, even if unconformities are not visible.

graded. The sedimentary packages bounded by the u2, u3 and u5 unconformities may also be interpreted as two other halokinetic sequences (Fig. 10).

The TrackDip method suggests that parabreccias and slumps resulted from sliding along the flanks during diapir growth, as these beds display internal structures with tilt axes roughly parallel to the diapir. This suggests that each package of turbidites overlying parabreccias may correspond to halokinetic sequence. Therefore, from 207 to 235 m, four additional halokinetic sequences may be defined, even though angular unconformities were not observed (Fig. 10). Below the Punta de Bakio unit, in the upper part of the Bakio breccias Fm., there is no clear repetition of such sedimentary packages (Fig. 4), suggesting the dominance of chaotic gravitational processes. Each parabreccia bed and its overlying marls may correspond to a halokinetic sequence. Stacked parabreccia beds may be interpreted as the result of a high repetition of thin halokinetic sequences, with erosion or reworking of the upper part of the underlying sequences.

Lateral facies variations are found within the halokinetic sequences (Fig. 10). Parabreccias are more abundant and relatively thicker near the diapir (Fig. 10). On the contrary, siliciclastic turbidite facies are thicker away from diapir (Fig. 10). Parabreccias probably wedge out away from the diapir, whereas turbidites onlap on the diapir. These geometries are consistent with slumping and currents directions found in 6.4 section (Fig. 8a), as turbidites proceeded from the North, whereas slumps and parabreccias were triggered by diapir growth.

In the eastern wedge, breccias are almost absent in the Sollube unit (Fig. 4). According to the halokinetic sequences model, the diapir may be buried and gravity-driven deposits are absent, when sedimentation exceeds the diapir rise. As the Sollube unit is up to 1500 m thick, SE of Bakio (Vicente-Bravo & Robles, 1991a), this suggests high sedimentation rates for this unit. Therefore, the Sollube unit probably onlapped on and buried the eastern diapir flank.

Tertiary shortening

In the Punta de Bakio outcrops, bedding planes in the Jata unit are horizontal, *ca.* 700 m away from the diapir. This points out that flanks tilting only affects a limited area around the diapir. Farther SW, more than 2 km away from the diapir, the Jata unit is dipping *ca.* 45° westward, indicating that deformation of this unit in this area is due to later Pyrenean folding and not to Bakio diapir uplift.

Mesoscale folds are found around the Bakio diapir with folds axes plunging westward in the western flank and eastward in the eastern flank, respectively, suggesting tilting of these axes by salt rise after Pyrenean folding. Bedding planes in both diapir flanks are overturned and dip towards each other (Fig. 3b). This geometry may be related to slight Tertiary shortening through the diapir.

DISCUSSION

This section provides a discussion of the chronology of the Bakio diapir emplacement, its impact on carbonate platform development and the velocity of diapir growth. It finally addresses a discussion on drag folds and drape and halokinetic sequence models.

Timing and heterogeneities of the Bakio diapir growth

The oldest unit tilted by diapir growth is the Bakio marls unit (Early Albian). The oldest evidence of diapir growth is the u1 unconformity top of the Bakio marls unit (Fig. 4), as there is neither thinning of this unit towards the diapir nor angular unconformities. The u1 unconformity is located where the Gaztelugatxe fault connects to the diapir, thus it is difficult to decipher whether the dip of the Bakio marls unit is due to diapir growth, faulting or both. The youngest evidence for diapir rising in the western flank is the unconformity at the base of the Jata unit (Late Albian) overlying the Bakio breccias Fm. (Fig. 4). Therefore, the diapir rose at least since deposition of the Bakio breccias Fm. until deposition of base of the Jata unit, i.e. from early Middle Albian (*dentatus* Zone) to Late Albian times.

All tilt axes of the wedges are oblique to the diapir axis and are roughly convergent northward (Fig. 8a). Both diapir flanks are also convergent northward, indicating that the diapir may be a conic, salt-cored antiform. Convergent tilt axes suggest that the diapir acquired this geometry during sedimentation, probably due to diachronic lateral migration of diapir growth.

In the western flank, the source area for gravity-driven deposits including parabreccias is the diapir roof, as slump with limestones blocks derived from the diapir. This implies the development of a carbonate platform top of the Bakio diapir, probably due to shallowing and creation of topographical high on the sea floor (Fig. 11a). Blocks in breccias exhibit similar facies in both the western diapir flank and the footwall of the Gaztelugatxe fault and the apex of the diapir connected with the footwall of the fault (Fig. 11a). This suggests that a single carbonate platform developed top of the diapir and the footwall of the Gaztelugatxe fault.

In the southern part of the Bakio diapir, only marls and rare thin-bedded grainstones are found as lateral equivalents to breccias, only located in the northern part of the diapir. This suggests higher rates of salt flow to the north, or that salt uplift began earlier in the north. This may explain the conical geometry of the diapir.

In the western flank, angular unconformities within the Punta de Bakio unit and at its top attest that the diapir growth lasted during the Late Albian in this area. In the Gaztelugatxe Island, flows recorded by turbidites of the Sollube unit flowed roughly southward (Fig. 8a), without being driven by any significant relief, indicating that the

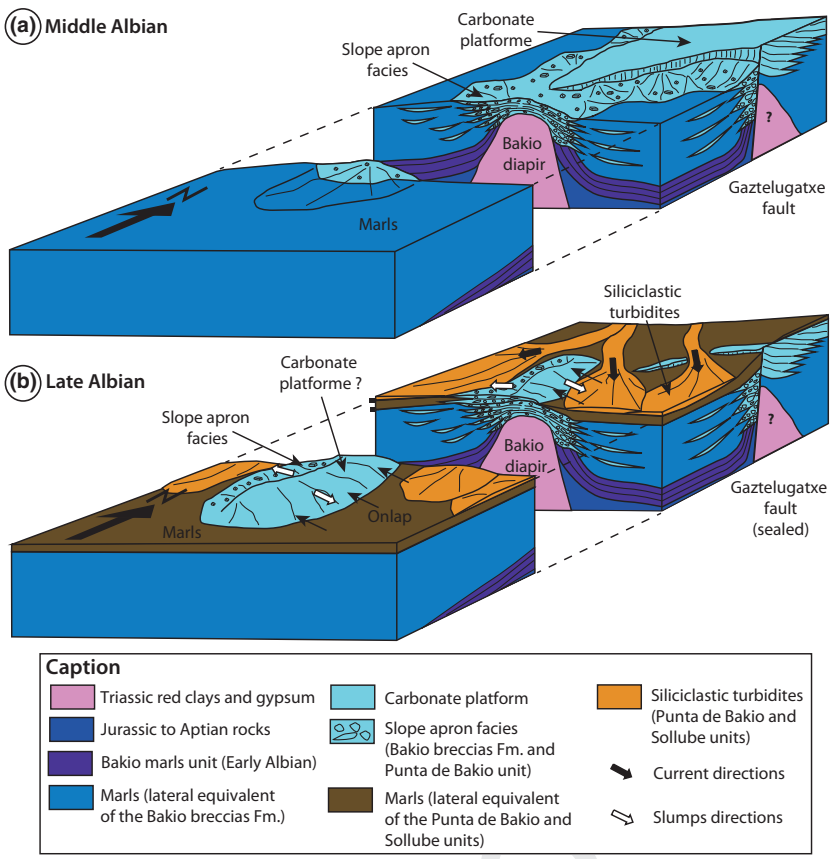

Fig. 11. Schematic 3D diagrams of the Bakio diapir during early Middle Albian (a) and Late Albian (b). (a) Initiation of the Bakio diapir as a reactive diapir in response to the offset of the Gaztelugatxe fault during early Middle Albian. (b) Passive stage of diapir growth during Late Albian.

Gaztelugatxe fault was buried at this time. In the eastern flank, the Sollube unit gravity-driven breccia deposits are almost absent. This suggests that the Sollube unit probably also onlapped on and buried the eastern flank of the diapir (Fig. 11b), as high sedimentation rate exceeded those of diapir rise. Westward migration of salt may be related to differential loading on the initial salt layer, in the eastern flank, produced by the Sollube unit, which is up to 1500 m thick, SE of Bakio (Vicente-Bravo & Robles, 1991a).

Such results, together with the conical geometry of the diapir, suggest diachronic lateral migration of diapir growth. As the diapir and the Gaztelugatxe fault probably initiated together during the early Middle Albian, the diapir is interpreted as a reactive diapir growing in response to the offset of the fault (Fig. 11a). Movements of the Gaztelugatxe fault ceased, while the diapir continued to rise at least until deposition of the Jata unit. Therefore, the Bakio diapir is assumed to have evolved passively, with south-westward migration of salt, during the Late Albian (Fig. 11b).

In the northern part of the Basque Country (including the Bakio area), Agirrezabala (1996) and García-Mondéjar *et al.* (1996) reported individualization of small troughs filled by Middle Albian coarse-grained gravity-driven deposits (like the Bakio breccias Fm.) separating paleo-highs with Urgonian carbonate platforms. These depocentres were bounded by normal NE–SW- and N–S-striking faults, suggesting a local E–W or NW–SE extension. The Bakio diapir and the Gaztelugatxe fault are both striking NE–SW and probably initiated in response to the local, E–W to NW–SE extension. In the Basque–Cantabrian Basin, NE–SW faults are commonly interpreted as inherited Hercynian faults (García-Mondéjar, 1996). The Bakio diapir and the Gaztelugatxe fault may be located above a basement fault striking NE–SW and may connect at depth with this latter. Reactivation of this basement fault by local NW–SE extension could have initiated the Bakio diapir growth during early Middle Albian times. Bodego & Agirrezabala (2013) document contemporaneous halokinetic deformations controlled by basement normal faulting in the north-eastern margin of the basin. Localization of diapirs above basement faults has been also reported in the Aquitaine Basin (Canérot *et al.*, 2005). López-Horgue *et al.* (2010) showed that the Pondra diapir (western Basque–Cantabrian Basin, see Fig. 2) also rose as a reactive diapir, in response to local NW–SE extension, during the Early Albian.

Finally, the Bakio area underwent a limited Tertiary deformation as most of Albian structures were not inverted or only slightly tilted. The latest south-eastward tilt of the Gaztelugatxe fault may be linked to Pyrenean shortening. Despite the Tertiary shortening, Albian structures remained first order structures.

Uplift rates of the diapir roof

In order to determine uplift rates of the diapir roof, an estimation of the entire Albian tilt angle is needed for the wedges (as explain in the Methods section). For the Bakio

diapir, the entire tilt angle of each wedge may result of a combination of Albian tilts and Pyrenean shortening. The addition of angles between unconformities and the underlying tilted sediments have been used, rather than the entire tilt angle for each wedge, in order to exclude possible Pyrenean tilt. Assuming that sedimentary surfaces were initially close to horizontal, addition of angles is supposed to correspond to tilts that occurred during sedimentation. As schistosity is absent in the study area, these angles were probably not significantly affected by Pyrenean shortening.

However, sedimentation surfaces were not horizontal in all cases because several surfaces around the diapir correspond to scars resulting from sliding along dipping slopes. It is not possible to accurately determine the initial dip of these erosional surfaces. Because of their transport as flows, turbidites are supposed to be deposited on sub-horizontal slopes. On the contrary, mass deposits can develop on relatively dipping slopes (not higher than 10° in submarine environments). Therefore, the estimation of the tilt angle between unconformity and underlying tilted beds is better when unconformities are overlaid by turbidites rather than mass deposits. When sediments deposited over angular unconformities are mass deposits, the angle between erosional surface and underlying tilted sediments may be underestimated (up to 10°).

In the eastern flank, the s1 unconformity represents a 54° tilt between the underlying and overlying sediments. As the overlying sediments are composed of breccias, the tilt angle may be underestimated. In the western flank, there are four angular unconformities developed in the Punta de Bakio wedge (u2, u3, u4 and u5, from 234 to 267 m). The measured tilt for u2 and u3 unconformities are 7° and 17° respectively. It was not possible to acquire measurement of bedding planes orientation between the u4 and u5 unconformities, but comparison from below u4 and above u5 unconformities gives an estimated angle of 14°. The addition of these angles gives a total angle of 38°. This value is similar to the tilt no. 1, with a tilt angle of 35° (Fig. S1).

As explained in the Methods section, calculation of tilt angles allows estimation of the diapir roof uplift rate, as biostratigraphical data are available within synkinematic strata. In this study, only a range from two extreme values can be estimated due to poor biostratigraphical constraints. In the eastern flank, the tilt (54°) occurred after deposition of the Bakio marls unit (Early Albian) and before deposition of the Bakio breccias Fm. (*dentatus* Zone) in a time span about 1 Myr or less (based on the geological timescale of Ogg & Hinnov, 2012). In the western flank, the tilt (38°) occurred during deposition of the upper part of the Bakio breccias Fm. and of the Punta de Bakio unit, and thus may have lasted 1.5 Myr. It gives a range of the diapir roof uplift rates from 0.36 to 6.8 mm a^{-1}. As explained above in the Methods section, such values may have different significations. If the diapir is buried, the values correspond to the diapir roof uplift rate and approximately equal the salt flow velocity. If salt reaches the surface, these values represent only the uplift rate of the edge of the diapir as the salt flow velocity may be higher. In the Bakio area, there is no evidence of emergence of salt during sedimentation, as salt tongues or Triassic clasts within deposits from the overburden are absent. Therefore, the range of uplift rates and salt flow velocity may be approximately equal.

In the literature, rates of salt flow and uplift are estimated using various methods. For example, Talbot & Jarvis (1984) and Talbot & Aftabi (2004) postulated simple hypotheses in which the salt flow velocity is only driven by the weight and the density of the overburden. These authors provided an equation for calculation of salt flow velocity. They found values from 82 mm a^{-1} (Talbot & Aftabi, 2004) to 170 mm a^{-1} (Talbot & Jarvis, 1984) for salt flow velocity for two diapirs in Iran. Frumkin (1996) used radiochronological dating on Neogene–Pleistocene uplifting salt from the Dead Sea and obtained values from 6 to 7 mm a^{-1} for salt flow velocity. Pirazzoli *et al.* (2004) used radiochronological dating on uplifted coral reef Quaternary marine terraces, developed top of diapirs from the Iranian coast and calculated an uplift of diapir roof equal to 2 mm a^{-1}. Aftabi *et al.* (2010) estimated salt flow velocity from 511 mm a^{-1}, also from another Iranian diapir, using InSAR mapping.

The large discrepancies of the values, different methods, timescales of observations and geological contexts make the comparison between these studies difficult. The different timescales of observations are an important unsolved problem to compare these data. For example, rates of salt flow recorded with InSAR represent punctual measurements (14 years for Aftabi *et al.*, 2010) compared to the results of this study (*ca.* 1.5 Myr). Since salt flow velocity is considered to change rapidly over short periods of time, as proposed by the halokinetic sequence model (Giles & Lawton, 2002; Rowan *et al.*, 2003), short-term results may represent pulses of salt growth whereas long-term results are likely to be time average.

If this problem of timescales of observations is neglected, a trend of diapirs with fast (>10 mm a^{-1}) and slow (<10 mm a^{-1}) rates of salt flow may be defined. The results of this paper are similar to those of Frumkin (1996) and Pirazzoli *et al.* (2004) with relatively slow motions compared to other studies (Talbot & Jarvis, 1984; Talbot & Aftabi, 2004; Aftabi *et al.*, 2010). It may be argued that the geological context drastically influence rates of salt flow as Iranian diapirs studied by Talbot & Jarvis (1984), Talbot & Aftabi (2004) and by Aftabi *et al.* (2010) show faster rates of salt flow. It may be related to important shortening occurring in the Zagros Montain. On the contrary, diapirs with slow rates of salt flow (or diapir roof uplift) from Bakio (this study), the Dead Sea (Frumkin, 1996) and the Persian Gulf (Pirazzoli *et al.*, 2004) developed on subsiding areas. Moreover, in diapirs with fast rate of salt flow (Talbot & Jarvis, 1984; Talbot & Aftabi, 2004; Aftabi *et al.*, 2010), salt reaches surface and flows upward rapidly which was probably not the case for

the Bakio diapir. In addition, diapirs with fast rates of salt flow are developed in continental area and are submitted to dissolution by rainfall as salt emerged at surface. Dissolution of salt top of diapirs may considerably increase salt velocity flow. The comparison between these studies suggests that diapirs with fast (>10 mm a^{-1}) salt velocity flow may develop in continental areas with important shortening, with salt emerging at surface, submitted to dissolution by rainfall. On the contrary, diapirs with slow (<10 mm a^{-1}) salt velocity flow rather develop in subsiding areas and are probably buried. This was probably the case of the Bakio diapir.

In this study, sparse biostratigraphical data do not allow an accurate estimation of velocity of diapir growth. However, the estimation of uplift rate of the diapir roof, constrained by accurate biostratigraphical data may be a novel approach to constraining rates of halokinesis in other diapirs. This method may be useful to demonstrate changes of rate over time and thus demonstrate relative growth rates between halokinetic sequences. Further investigation is still needed around the Bakio diapir to provide better biostratigraphical data, in order to refine the range of velocity of diapir growth.

Drag folds vs. drape folds

Structures in the overburden of the Bakio diapir are mainly angular unconformities, sedimentary wedges and slumps, indicating that deformation occurred at sea floor. Tilt axes of the slumps and wedges are parallel to the diapir trend (Fig. 8) and thus are clearly related to diapir rise. Major angular unconformities indicate that wedge tilting affected the sea floor (Fig. 6). The TrackDip results demonstrate that flank tilting with deformation occurring at the sea floor may explain most of the tilts within the western wedge. Slumps and parabreccias imply a dipping slope and significant relief related to the diapir apex. Such relief on the sea floor is confirmed by paleocurrent directions around the Bakio diapir, as the turbidity currents were driven by the diapir relief (Fig. 8a).

By contrast, most of faults affecting the overburden are related to regional tectonics and not to diapir growth. This suggests the absence of significant brittle deformation linked to diapir growth in the overburden. This suggests that most of deformation caused by diapir growth occurred in poorly consolidated sediments.

These results are not compatible with drag fold model (Jackson & Talbot, 1991; Jackson *et al.*, 1994; Alsop *et al.*, 1995, 2000; Alsop, 1996), as this model cannot explain different upturn degrees separated by unconformities in the wedges. Wedges with overturned beds, angular unconformities and slumps around the Bakio diapir are similar to those described by Giles & Lawton (2002) and Rowan *et al.* (2003) from the El Papalote diapir (Fig. 1c). Diapir growth related deformation occurred near or at surface and not at depth, therefore this support the drape fold model.

Halokinetic sequences

In the western diapir flank, the data show that slumps are triggered by tilting the sea floor during diapir growth. These slumps are composed of folded grainstones and orthobreccia beds and limestones blocks within a marly matrix. Parabreccia beds display the same types of clasts and matrix, which suggests a genetic relationship with the slumps. Downslope flow transformation of slump to parabreccias may be inferred, regarding the similitude in clasts and matrix. Therefore, parabreccias are assumed to result of mud-supported debris flows derived from the diapir roof.

Slumps and parabreccias are interbedded with turbidites and marls indicating episodic production of slumps and mud-supported debris flows by slope failure. Paleocurrent and slumping directions around the Bakio diapir indicate multi-source system with slumps and parabreccias triggered by diapir rise, and turbidity flows coming from the Landes Massif (Fig. 8a). Parabreccias alternating with turbidites suggest episodic changes in direction of sedimentary transport, together with a change in sedimentary processes. Packages composed of parabreccias in the lower part and thin-bedded fine-grained turbidites in the upper part, separated by unconformites, can be defined in the Punta de Bakio stratigraphical section (Fig. 10). These packages have similar thickness from 4 to 12 m (Fig. 10), indicating cyclic repetition of slope failure.

Such sedimentary packages, composed of parabreccias alternating with turbidites, are interpreted as halokinetic sequences as diapir growth causes cyclic repetition of slope failure as described by Giles & Lawton (2002) and Rowan *et al.* (2003). According to the halokinetic sequences model, when rates of sedimentation are low relative to those of salt rise, tilted sediments on diapir flanks reach slope failure, slide, and gravity-driven deposits develop at the toe of the slope. When rates of sedimentation are high relative to those of salt rise, onlap on the flanks prevent sediments to reach slope failure. In the Punta de Bakio stratigraphical section, doming in the diapir crest (when diapir rising velocity >accumulation rate) triggered mud-supported debris flows, forming the lower part of halokinetic sequences. Turbidites constituting the upper part of halokinetic sequences, came from the north and onlapped the slope previously formed (when diapir rising <accumulation rate). Such interaction between gravity-driven deposits triggered by diapir growth and regional deposits may be found in other diapirs, if the input of regional sediments is independent of diapir growth.

The halokinetic sequences from the western wedge are characterized by low-angle unconformities (u2–u6) and are associated with broad zone of drape folding (*ca.* 700 m), thus may correspond to wedge halokinetic sequence as described by Giles and Rowan (2012). In the eastern flank, the u1 major unconformity shows a high tilt

angle (54°) and may correspond to the basal part of a hook halokinetic sequence. According to Giles and Rowan (2012), wedge and hook halokinetic sequences are found when sedimentation rates are superior and inferior to the rates of diapir rise respectively. In the Basque Trough, the onset of siliciclastic turbidite deposition, during the Late Albian, coincides with an increase in sedimentation rates as the Black Flysch units may be 7000 m thick (Martín-Chivelet *et al.*, 2002; García-Mondéjar *et al.*, 2004). Therefore, prior to the Late Albian, the Bakio diapir growth probably produced hook halokinetic sequences, as suggested by the u1 unconformity and the lower sedimentation rates. Then, during the Late Albian, diapir growth produced wedge halokinetic sequences because of the high sedimentation rates associated with siliciclastic turbidites deposition. It demonstrates that the hook and wedge halokinetic sequences model is relevant for the Bakio diapir.

CONCLUSIONS

The Bakio diapir and its overburden provide new important data from an outcrop case with syndiapir growth strata, well-exposed sedimentary wedges, major unconformities and upturned strata. The study of this diapir brings new key elements for (i) local understanding of the timing of diapir growth, which was previously unknown, (ii) insights for the drape folds and (iii) halokinetic sequences models and offers (iv) a new method for estimating rates of diapir growth. These new key elements are listed below:

(i)The Bakio diapir probably initiated during the early Middle Albian as a reactive diapir in response to the offset of the Gaztelugatxe fault, and evolved passively from Middle to Late Albian times. Rate of diapir growth was variable through times, as salt probably started rising north of Bakio during the early Middle Albian and then preferentially southward, when movements of the Gaztelugatxe fault ceased during the Late Albian. The range of rates of salt rise is estimated from 0.36 to 6.8 mm a^{-1} during the passive stage of the diapir. During the Tertiary shortening, linked to the Pyrenean orogeny, the diapir was probably gently reactivated.
(ii)Structural data and analysis with the TrackDip method show deformation at the sea floor and absence of shear generated by salt flow at depth in the overburden. This demonstrates the relevance of the drape fold model for the Bakio diapir, yet the drag fold model is not suitable. This conclusion may be valid for other diapir beyond the La Popa Basin. Further studies on other diapirs are still needed to confirm this hypothesis.
(iii)Unconformity-bounded sedimentary packages composed of breccias in the lower part and turbidites interbedded with marls in the upper part are interpreted as wedge halokinetic sequences. This points out that the halokinetic sequences model described previously only for the La Popa basin, is relevant for the Bakio diapir and thus probably for other passive diapirs. In addition, this study illustrates how turbidites produced by flows emanating from another source are interbedded with gravity-driven deposits triggered by diapir growth. Such interplay between regional sediments and gravity-driven deposits may be found in other diapir, where the source of regional sediments is independent of diapir growth.
(iv)This work offers a new simple method for estimating the velocity of diapir growth, based on the estimation of the velocity of diapir flank tilting by dating synkinematic strata with biostratigraphical data. This method may be useful for other outcrop studies where biostratigraphical data are available.

ACKNOWLEDGEMENTS

The authors would like to thank the ARNT-CIFRE and Geolink, for the funding of the PhD work of Y. Poprawski. We gratefully acknowledge I. Alsop, N. Mountney and an anonymous reviewer for their interesting critics and comments that greatly improve the manuscript. We also like to thank M. Bernet for his help to improve the English language.

SUPPORTING INFORMATION

Additional Supporting Information may be found in the online version of this article:

Table S1. Results of the TrackDip method showing the major tilts for the largest window sizes.
Table S2. Results of the TrackDip method showing the tilts related to the s2 slumped interval.
Table S3. Results of the TrackDip method showing the tilts related to the s3 slumped interval.
Table S4. Results of the TrackDip method showing pair of tilts with opposing dip directions, related to small slumped structures.
Figure S1. (a) Bedding planes attitudes from the Punta de Bakio stratigraphical section and results from the TrackDip method (tilts for window size less than 10 m are not shown, see Fig. S2).
Figure S2. Details of several tilts that coincides on sedimentary structures as slumps and unconformities.

REFERENCES

Ábalos, B., Alkorta, A. & Iribar, V. (2008) Geological and isotopic constraints on the structure of the Bilbao Anticlinorium (Basque-Cantabrian Basin, north Spain). *J. Struct. Geol.*, **30**, 1354–1367.

Aftabi, P., Roustaie, M., Alsop, G.I. & Talbot, C.J. (2010) InSAR mapping and modelling of an active Iranian salt extrusion. *J. Geol. Soc.*, **167**, 155–170.

Agirrezabala, L.M. 1996. El Aptiense-Albiense del Anticlinorio Nor-Vizcaino entre Gernika y Azpeitia. PhD Thesis, Euskal Herriko Unibertsitatea, Bilbo, 429 pp.

Agirrezabala, L.M. & García-Mondéjar, J. (1989) EvoluciÓn tectosedimentaria de la plataforma urgoniana entre Cabo OgoÑo e Itziar (Aptiense-Albiense superior, RegiÓn vasco-cantabrica oriental). In: *Syrnposium, XIZ Congreso EspaÑol de Sedimentologia* (Ed. by S. Robles, J. García-Mondéjar, A. Garrote), pp. 11–20. UPV & EVE, Bilbao.

Alsop, G.I. (1996) Physical modelling of fold and fracture geometries associated with salt diapirism. In: *Salt Tectonics* (Ed. by Alsop G.I., Blundell D.J. & Davison I.) *Geol. Soc. (London) Spec. Publ.*, **100**, 227–241.

Alsop, G.I. & Marco, S. (2011) Soft-sediment deformation within seismogenic slumps of the Dead Sea Basin. *J. Struct. Geol.*, **33**, 433–457.

Alsop, G.I., Jenkins, G. & Davison, I. (1995). A preliminary study of drag zone geometry adjacent to salt diapirs, in Salt, sediment and hydrocarbons. Gulf Coast Section, SEPM 16th Annual Research Conference, p. 1–9.

Alsop, G.I., Brown, J.P., Davison, I. & Gibling, M.R. (2000) The geometry of drag zones adjacent to salt diapirs. *J. Geol. Soc. (London)*, **157**, 1019–1029.

Banham, S.G. & Mountney, N.P. (2013a) Evolution of fluvial systems in salt-walled minibasins: a review and new insights. *Sed. Geol.*, ???, ???–???. 9

Banham, S.G. & Mountney, N.P. (2013b) Climatic versus halokinetic control on sedimentation in a dryland fluvial succession: Triassic Moenkopi Formation, Utah, USA. *Sedimentology*, ???, ???–???. 10

Banham, S.G. & Mountney, N.P. (2013c) *Controls on fluvial sedimentary architecture and sediment-fill state in salt-walled mini-basins: Triassic Moenkopi Formation, Salt Anticline Region, SE Utah*. Basin Research, USA.

Barton, D.C. (1933) Mechanics of formation of salt domes with special reference to Gulf Coast salt domes of Texas and Louisiana. *Am. Assoc. Pet. Geol. Bull.*, **17**, 1025–1083.

Basile, C., Pecher, A., Corazzi, M., Odonne, F., Maillard, A., Debroas, E.J. & Callot, P. (2009) TrackDip: a multi-scale processing of dipmeter data – method, tests, and field example for 3-D description of gravity-driven deformations in the Eocene foreland basin of Ainsa, Spain. *Mar. Pet. Geol.*, **26**, 738–751.

Bodego, A. & Agirrezabala, L.M. (2013) Syn-depositional thin- and thick-skinned extensional tectonics in the mid Cretaceous Lasarte sub-basin, western Pyrenees. *Basin Res.*, **25**. doi:10.1111/bre.12017

Canérot, J., Hudec, M. & Rockenbauch, K. (2005) Mesozoic diapirism in the Pyrenean orogen: salt tectonics on a transform plate boundary. *Am. Assoc. Pet. Geol. Bull.*, **89**, 211–229.

Davison, I., Alsop, I., Birch, P., Elders, C., Evans, N., Nicholson, H., Rorison, P., Wade, D., Woodward, J. & Young, M. (2000) Geometry and late-stage structural evolution of Central Graben salt diapirs, North Sea. *Mar. Pet. Geol.*, **17**, 499–522.

Frumkin, A. (1996) Uplift rate relative to base-levels of a salt diapir (Dead Sea basin, Israel) as indicated by cave levels. *Geol. Soc. London Spec. Publ.*, **100**, 41–47.

García-Mondéjar, J. (1996) Plate reconstruction of the Bay of Biscay. *Geology*, **24**(7), 635–638.

García-Mondéjar, J. & Robador, A. (1986-1987) Sedimentación y paleogeografía del Complejo Urgoniano (Aptiense-Albiense) en el area de Bermeo (region Vasco-CantÁbrica septentional). *Acta GeolÓgica HispÁnica*, **t. 21-22**, 411–418.

García-Mondéjar, J., Agirrezabala, L.M., Aranburu, A., Fernández-Mendiola, P.A., Gómez-Pérez, I., López-Horgue, M.A. & Rosales, I. (1996) The Aptian-Albian tectonic pattern of the Basque-Cantabrian Basin (northern Spain). *Geol. J.*, **31**, 13–45.

García-Mondéjar, J., Fernández-Mendiola, P.A., Agirrezabala, L.M., Aranburu, A., López-Horgue, M.A., Iriarte, E. & Martinez de Rituerto, S. (2004) El Aptiense-Albiense de la Cuenca Vasco-CantÁbrica. En: *GeologÍa de EspaÑa* (Ed. by ?. ????????), pp. 291–296. SGE-IGME, ??????????. 11

Giles, K.A. & Lawton, T.F. (2002) Halokinetic sequence stratigraphy adjacent to the El Papalote diapir, northeastern Mexico. *Am. Assoc. Pet. Geol. Bull.*, **86**, 823–840.

Gómez, M., Vergés, J. & Riaza, C. (2002) Inversion tectonics of the northern margin of the Basque Cantabrian Basin. *Bulletin de la SociÉtÉ GÉologique de France*, **173**(5), 449–459.

Handy, M.R., Schmid, S.M., Bousquet, R., Kissling, E. & Bernoulli, D. (2010) Reconciling plate-tectonic reconstructions of Alpine Tethys with the geological-geophysical record of spreading and subduction in the Alps. *Earth Sci. Rev.*, **102**, 121–158. 12

Hudec, M.R., Jackson, M.P. & Schultz-Ela, D.D. (2009) The paradox of minibasin subsidence into salt: clues to the evolution of crustal basins. *Geol. Soc. Am. Bull.*, **121**, 201–221.

Ings, S.J. & Beaumont, C. (2010) Shortening viscous pressure ridges, a solution to the enigma of initiating salt 'withdrawal'minibasins. *Geology*, **38**, 339–342.

Jackson, M.P.A. & Talbot, C.J. (1991) A glossary of salt tectonics. University of Texas at Austin, Bureau of Economic Geology Geological Circular No. 91-4, 44.

Jackson, M.P.A., Vendeville, B.C. & Schultz-Ela, D.D. (1994) Structural dynamics of salt systems. *Annu. Rev. Earth Planet. Sci.*, **22**, 93–117.

Jackson, M.P.A., Shultz-Ela, D.D., Hudec, M.R., Watson, I.A. & Porter, M.L. (1998) Structure and evolution of Upheaval Dome: a pinched-off salt diapir. *Geol. Soc. Am. Bull.*, **110**(12), 1547–1573.

López-Horgue, M.A., Owen, H.G., Aranburu, A., Fernández-Mendiola, P.A. & García-Mondéjar, J. (2009) Early late Albian (Cretaceous) of the central region of the Basque-Cantabrian Basin, northern Spain: biostratigraphy based on ammonites and orbitolinids. *Cretac. Res.*, **30**, 385–400.

López-Horgue, M.A., Iriarte, E., Schröder, S., Fernández-Mendiola, P.A., Caline, B., Corneyllie, H., Frémont, J., Sudrie, M. & Zerti, S. (2010) Structurally controlled hydrothermal dolomites in Albian carbonates of the Ason valley, Basque Cantabrian Basin, northern Spain. *Mar. Pet. Geol.*, **27**, 1069–1092.

Martín-Chivelet, J., *et al.* (2002) Cretaceous. In: *The Geology of Spain* (Ed. by W. Gibbons & T. Moreno), pp. 255–292, Geological Society of London, ???????. 13, 14

Mutti, E. & Davoli, G. (1992) *Turbidite Sandstones*. Agip, Istituto di geologia, UniversitÀ di Parma, ???????, 275 pp. 15, 16

Nelson, T.H. (1991) Salt tectonics and listric normal faulting. In: *The Gulf of Mexico Basin (The Geology of North America, J.)* (Ed. by A. Salvador), pp. 73–89. Geological Society of America, Boulder, CO.

Ogg, G.J. & Hinnov, L.A. (2012) Cretaceous. In: *The Geologic Time Scale* (?. ????????), pp. 793–853. Elsevier, ?????????.

Olivet, J.-L. (1996) Kinematics of the Iberian plate. *Bulletin des Centres de Recherches Exploration-Production Elf Aquitaine*, **20**, 131–195.

Pirazzoli, P.A., Reyss, J.L., Fontugne, M., Haghipour, A., Hilgers, A., Kasper, H.U., Nazari, H., Preusser, F. & Radtke, U. (2004) Quaternary coral-reef terraces from Kish and Qeshm Islands, Persian Gulf: new radiometric ages and tectonic implications. *Quatern. Int.*, **120**, 15–27.

Rat, P. (1988) The Basque-Cantabrian Basin between the Iberian and the European Plates. Some facts but still many problems. *Revista de la Sociedad de Geologia de EspaÑa*, **1**, 3–4.

Robles, S., Pujalte, V. & García-Mondéjar, J. (1988) EvoluciÓn de los sistemas sedimentarios del margen continental cantÁbrico durante el Albiense y Cenomaniense, en la transversal del litoral vizcaino. *Revista de la Sociedad de Geologia de EspaÑa*, **1**(3–4).

Rosenbaum, G., Lister, G.S. & Duboz, C. (2002) Relative motions of Africa, Iberia and Europe during Alpine orogeny. *Tectonophysics*, **359**, 117–129.

Rowan, M.G., Lawton, T.F., Giles, K.A. & Ratliff, R.A. (2003) Near-salt deformation in La Popa basin, Mexico, and the northern Gulf of Mexico: a general model for passive diapirism. *Am. Assoc. Pet. Geol. Bull.*, **87**, 733–756.

Schultz-Ela, D.D. (2003) Origin of 'drag' folds bordering salt diapirs. *Am. Assoc. Pet. Geol. Bull.*, **87**, 757–780.

Sibuet, J.C., Srivastava, S.P. & Spakman, W. (2004) Pyrenean orogeny and plate kinematics. *J. Geophys. Res.*, Washington, **109**, ???–???.

Stewart, S.A. (2006) Implications of passive salt diapir kinematics for reservoir segmentation and radial and concentric faults. *Mar. Pet. Geol.*, **23**, 843–853.

Talbot, C. & Aftabi, P. (2004) Geology and models of salt extrusion at Qum Kuh, central Iran. *J. Geol. Soc.*, **161**, 321–334.

Talbot, C.J. & Jarvis, R.J. (1984) Age, budget and dynamics of an active salt extrusion in Iran. *J. Struct. Geol.*, **6**, 521–533.

Vendeville, B.C. & Jackson, M.P.A. (1992) The rise of diapirs during thin-skinned extension. *Mar. Pet. Geol.*, **9**, 331–353.

Vendeville, B.C. & Jackson, M.P.A. (1993) Some dogmas in salt tectonics challenged by modeling (abs.). American Association of Petroleum Geologists Hedberg International Research Conference on Salt Tectonics, Bath, England, September 1993, p. 263–265.

Vicente-Bravo, J.C. & Robles, S. (1991a) GeometrÍa y modelo deposicional de la secuencia Sollube del Flysch Negro (Albiense medio, norte de Bizkaia). *Geogaceta*, **10**, 69–72.

Vicente-Bravo, J.C. & Robles, S. (1991b) CaracterizaciÓn de las facies de la transiciÓn canal-lobulo en la secencia Jata del Flysch Negro (Albiense Superior, Norte de Vizcaya). *Geogaceta*, **10**, 72–75.

Vicente-Bravo, J.C. & Robles, S. (1995) Large-scale mesotopographic bedforms from the Albian Black Flysch, northern Spain: characterization, setting and comparisons with recent analogues. In: *Atlas of Deep Water Environments: Architectural Style in Turbidite Systems* (Ed. by K.T. Pickering, R.N. Hiscott, N.H. Kenyon, F. Ricci Lucchi & R.D.A. Smith), pp. 216–226. Chapman & Hall, London.

Voort, H.B. (1963) Zum flysch problem in den WestpyrenÄen. *Geol. Rundsch.*, **53**, 220–233.

Weijermars, R., Jackson, M.P.A. & Vendeville, B.C. (1993) Rheological and tectonic modelling of salt provinces. *Tectonophysics*, **217**, 143–174.

Wiedmann, J. & Boess, J. (1984) Ammoniten funde aus der Biskaya-synkline (Nordspanien)-Kreidegliederung und Alter des Kreide-Vulkanismus. *Eclogae Geol. Helv.*, **77**, 483–510.

Manuscript received 27 March 2013; In revised form 13 January 2014; Manuscript accepted 22 January 2014.